Journal of Experimental Botany
https://doi.org/10.1093/jxb/erae119 Advance Access Publication 16 March 2024

RESEARCH PAPER

A tomato B-box protein regulates plant development and fruit quality through the interaction with PIF4, HY5, and RIN transcription factors

Lumi Shiose[1,†], Juliene dos Reis Moreira[1,†], Bruno Silvestre Lira[1], Gabriel Ponciano[1], Gabriel Gómez-Ocampo[2], Raquel Tsu Ay Wu[1], José Laurindo dos Santos Júnior[1], Nikolaos Ntelkis[3,4], Elke Clicque[3,4], Maria José Oliveira[1], Greice Lubini[5], Eny Iochevet Segal Floh[1], Javier Francisco Botto[2], Marcelo José Pena Ferreira[1], Alain Goossens[3,4], Luciano Freschi[1], and Magdalena Rossi[1,*]

[1] Departamento de Botânica, Instituto de Biociências, Universidade de São Paulo, Rua do Matão 277, 05508-090, São Paulo, Brasil
[2] IFEVA, Facultad de Agronomía, Universidad de Buenos Aires y Consejo Nacional de Investigaciones Científicas y Técnicas, Avenida San Martín 4453, Buenos Aires C1417DSE, Argentina
[3] Department of Plant Biotechnology and Bioinformatics, Ghent University, Technologiepark-Zwijnaarde 71, Ghent, Belgium
[4] Center for Plant Systems Biology, VIB, Technologiepark-Zwijnaarde 71, Ghent, Belgium
[5] Departamento de Biologia, Faculdade de Filosofia, Ciências e Letras de Ribeirão Preto, Universidade de São Paulo, Avenida Bandeirantes 3900, 14040-901, Ribeirão Preto, Brasil

[†] These authors contributed equally to this work.
* Correspondence: mmrossi@usp.br

Received 4 December 2023; Editorial decision 8 March 2024; Accepted 15 March 2024

Editor: Sonia Osorio, University of Malaga, Spain

Abstract

During the last decade, knowledge about BBX proteins has greatly increased. Genome-wide studies identified the *BBX* gene family in several ornamental, industry, and food crops; however, reports regarding the role of these genes as regulators of agronomically important traits are scarce. Here, by phenotyping a knockout mutant, we performed a comprehensive functional characterization of the tomato locus Solyc12g089240, hereafter called *SlBBX20*. The data revealed the encoded protein as a positive regulator of light signaling affecting several physiological processes during the life span of plants. Through inhibition of PHYTOCHROME INTERACTING FACTOR 4 (SlPIF4)–auxin cross-talk, SlBBX20 regulates photomorphogenesis. Later in development, it controls the balance between cell division and expansion to guarantee correct vegetative and reproductive development. In fruits, SlBBX20 is transcriptionally induced by the master transcription factor RIPENING INHIBITOR (SlRIN) and, together with ELONGATED HYPOCOTYL 5 (SlHY5), up-regulates flavonoid biosynthetic genes. Finally, SlBBX20 promotes the accumulation of steroidal glycoalkaloids and attenuates *Botrytis cinerea* infection. This work clearly demonstrates that BBX proteins are multilayer regulators of plant physiology because they affect not only multiple processes during plant development but they also regulate other genes at the transcriptional and post-translational levels.

Keywords: BBX proteins, hypocotyl elongation, light signaling, photomorphogenesis, plant defense, ripening, shade avoidance, *Solanum lycopersicum*, specialized metabolism, tomato.

Introduction

Initially characterized in *Arabidopsis thaliana* as pivotal factors in light signaling, plant BBX proteins have drawn attention during the last few years due to their involvement in several developmental processes, including seed germination, seedling photomorphogenesis, thermomorphogenesis, floral transition, shade avoidance, senescence, and even responses to biotic and abiotic stresses (Talar and Kiełbowicz-Matuk, 2021; Cao *et al.*, 2023). BBX proteins are zinc finger transcription factors (TFs) characterized by the presence of one or two B-box domains, which play a paramount role in protein–protein interaction. Additionally, some BBXs contain the CONSTANS, CONSTANS-LIKE, and TIMING OF CAB1 (CCT) domain in the C-terminus of the protein (Gangappa and Botto, 2014). The members of this protein family regulate transcription either by direct interaction with target gene promoters (Tiwari *et al.*, 2010; Xu *et al.*, 2016) or by modifying the transcriptional regulatory activity of other TFs through heterodimerization (Tripathi *et al.*, 2017; Song *et al.*, 2020).

Recently, genome-wide surveys have identified BBX protein-encoding genes in several economically important plant species, such as wild peanut *Arachis duranensis* (Jin *et al.*, 2019), sweet cherry (Y. Wang *et al.*, 2021a), *Gossypium* sp. (Feng *et al.*, 2021), *Iris germanica* (Y. Wang *et al.*, 2021b), cucumber (Obel *et al.*, 2022), rice/maize/sorghum/stiff brome/millet (Huang *et al.*, 2012; Shalmani *et al.*, 2019), potato (Talar *et al.*, 2017), apple (Liu *et al.*, 2018), orchid *Dendrobium officinale* (Cao *et al.*, 2019), grapevine (Wei *et al.*, 2020), pepper (Wang *et al.*, 2022), pear (Cao *et al.*, 2017), quinoa (Xuefen *et al.*, 2022), soybean (Shan *et al.*, 2022), *Saccharum spontaneum* (Wu *et al.*, 2023), sweet potato ancestor *Ipomoea trifida* (Hou *et al.*, 2021), *Nicotiana tabacum* (Song *et al.*, 2022), strawberry (Xu *et al.*, 2023a), yam (Chang *et al.*, 2023), and tomato (Lira *et al.*, 2020). However, the functional characterization of BBX proteins related to crop yield and quality traits remains scarce.

In tomato, out of the 31 BBX protein-encoding genes identified (Lira *et al.*, 2020), six were characterized as regulators of agronomically important traits. Beyond photomorphogenesis, SlBBX4 (Solyc08g006530) participates in the determination of flowering time, as evidenced by the higher number of leaves until the first anthesis observed in *Slbbx4* mutant genotype (Xu *et al.*, 2023b). Cui *et al.* (2022) demonstrated that SlBBX3/SlCOL1 (Solyc02g089540) affects yield by directly down-regulating the expression of *SINGLE FLOWER TRUSS* (*SlSFT*) florigen, consequently delaying flowering and reducing flower number. In contrast, SlBBX28 (Solyc12g005660) was found to be a positive regulator of flower and fruit number, acting downstream of SlSFT. By the up-regulation of auxin metabolism and transcriptional repression of *FRUITFULL2* (*SlFUL2*), SlBBX28 determines the proper inflorescence branching pattern. Moreover, SlBBX28-mediated auxin synthesis and signaling regulate vegetative growth (Lira *et al.*, 2022). Not only yield-related characters are regulated by SlBBXs, but also fruit quality traits, such as the content of nutraceutical compounds. In this sense, plants overexpressing *SlBBX25* (Solyc01g110180; although it was named *SlBBX20* by the authors, the locus corresponds to *SlBBX25* according to the first report of tomato BBX proteins, Chu *et al.*, 2016) developed dark green fruits and leaves, and ripe fruits with higher levels of carotenoids and flavonoids relative to its wild-type counterparts. Further experiments demonstrated that SlBBX25 modulates pigment accumulation in a light-mediated manner (Xiong *et al.*, 2019; Luo *et al.*, 2021). Finally, SlBBXs have also been shown to participate in the response to environmental biotic and abiotic cues. *SlBBX25* negatively regulates resistance to *Botrytis cinerea* (Luo *et al.*, 2023). *SlBBX17* (Solyc07g052620) is up-regulated by high temperature, and its overexpression confers heat tolerance with a dramatic gibberellin-mediated growth penalty (Xu *et al.*, 2022). *SlBBX17* expression is also induced by low temperatures conferring resistance in an ELONGATED HYPOCOTYL 5 (SlHY5)-dependent manner (Song *et al.*, 2023). Similarly, the overexpression of *SlBBX31* (Solyc07g053140) confers cold tolerance. Through a genome-wide association study in wild and cultivated tomato accessions, Zhu *et al.* (2023) discovered that an insertion of 27 bp in the promoter of *SlBBX31* that impairs SlHY5-mediated transcriptional induction in response to chilling temperatures has been negatively selected during domestication.

In a previous work, we characterized the expression profile of several *SlBBX* genes (Lira *et al.*, 2020). The mRNA levels of *SlBBX19* (Solyc01g110370), *SlBBX20* (Solyc12g089240), *SlBBX22* (Solyc07g062160), *SlBBX24* (Solyc06g073180), and *SlBBX26* (Solyc10g006750) increase from immature green towards red ripe stages of fruit development (Supplementary Fig. S1). *SlBBX20* shows the highest absolute expression and induction; moreover, its promoter binds RIPENING INHIBITOR (SlRIN), the master TF of tomato fruit ripening (Vrebalov *et al.*, 2002). Here, by a comprehensive phenotypic characterization of a knockout mutant, we demonstrate that SlBBX20 participates in light signaling, regulating several development processes, from seedling establishment to fruit ripening, positively impacting crop yield and fruit quality.

Materials and methods

Plant material and growth conditions

Solanum lycopersicum (cv. Micro-Tom) wild type (WT) harboring the wild allele of the *GOLDEN2-LIKE 2* (*SlGLK2*) gene (Nguyen *et al.*, 2014), and *Slrin* mutant genotypes were obtained from the Laboratory of hormonal control of plant development, University of São Paulo (https://www.esalq.usp.br/tomato/).

Nicotiana benthamiana and tomato plants were grown in 2 liter pots containing a 1:1 mixture of commercial substrate (Plantmax HT, Eucatex, Brazil) and vermiculite supplemented with 1 g l^{-1} NPK 10:10:10, 4 g l^{-1} dolomite limestone, and 2 g l^{-1} Yoorin Master® (Yoorin Fertilizantes, Brazil). Cultivation was carried out in a biosafety risk I greenhouse with manual irrigation by capillarity under controlled temperature (25 ± 3 °C day and 20 3 °C night) and natural light conditions [11.5 h/13 h photoperiod in winter/summer, respectively, and 250–350 μmol m^{-2} s^{-1} of incident photosynthetically active radiation (PAR)].

Subcellular localization and bimolecular fluorescence complementation

Subcellular localization was predicted using cNLS Mapper (https://nls-mapper.iab.keio.ac.jp, Kosugi *et al*., 2009), BaCelLo (http://gpcr.biocomp.unibo.it/bacello/, Pierleoni *et al*., 2006), and DeepLoc 2.0 (https://services.healthtech.dtu.dk/services/DeepLoc-2.0/; Thumuluri *et al.*, 2022).

The full-length ORF of *SlBBX20* (Solyc12g089240), *SlBBX26* (Solyc10g006750, as interaction negative control), *SlPIF4* (*PHYTOCHROME INTERACTING FACTOR 4*; Solyc07g043580), and *SlRIN* (Solyc05g012020) without a stop codon were amplified using specific primers listed in Supplementary Table S1, and were cloned into pCR™ 8/GW/TOPO TA Cloning (Invitrogen) entry vector. For subcellular localization, the *SlBBX20* coding region was recombined into the binary vector pK7FWG2 (Karimi *et al*., 2002) using LR clonase II enzyme mix (Invitrogen). Since SlBBX20 showed autoactivation when fused to the GAL4 DNA-binding domain of the yeast two-hybrid (Y2H) system, its homodimerization was assessed by bimolecular fluorescence complementation (BiFC) assay. *SlBBX20*, *SlBBX26*, *SlPIF4*, and *SlRIN* coding regions were recombined into pDEST-GWVYNE or pDEST-GWVYCE vectors (Gehl *et al*., 2009) using LR clonase II enzyme mix (Invitrogen). The binary vectors were introduced in *Agrobacterium tumefaciens* strain GV3101. Cultures were resuspended in infiltration buffer [50 mM MES pH 5.6, 2 mM sodium phosphate buffer pH 7, 0.5% glucose, and 200 μM acetosyringone (Sigma-Aldrich)] to a final OD_{600} of 0.5, incubated for 3 h in the dark at room temperature, and infiltrated into leaves of 4-week-old *Nicotiana benthamiana* plants. DAPI was used as a nuclear marker. Confocal analyses for subcellular localization and BiFC were carried out as described in Lira *et al*. (2017) in a Leica TCS SP8 STED 3X confocal system coupled to a Leica DMi 8 microscope (CAIMi IB-USP). GREEN FLUORESCENT PROTEIN (GFP) and YELLOW FLUORESCENT PROTEIN (YFP) signals were captured over a 508–553 nm range after excitation at 488 nm.

Generation of the *SlBBX20* CRISPR/Cas9 knockout line

Slbbx20 mutant tomato plants were obtained by the clustered regularly interspaced palindromic repeats (CRISPR)/CRISPR-associated protein 9 (CRISPR/Cas9) system in the *Solanum lycopersicum* (cv. Micro-Tom) background. Two guide RNA (gRNA) sequences were inserted into the pDIRECT_22C vector expressing the Csy4-multi-gRNA system (Čermák *et al*., 2017) to simultaneously target two sites in *SlBBX20* (Supplementary Table S1). Tomato plants were stably transformed with the construct via *A. tumefaciens*-mediated transformation according to Pino *et al*. (2010). The presence of the vector T-DNA was confirmed by PCR using primers: (i) TC320 and M13F anchored to the CmYLCV promoter and CSY terminator, respectively; and (ii) the Cas9 coding region (Supplementary Table S1). Cas9-mediated editions were analyzed in T_0 regenerated plants by PCR with BBX20-specific primers followed by Sanger sequencing (Supplementary Table S1). The T-DNA was segregated in the T_2 generation, and all experiments were performed with T_4 homozygous mutants.

Hypocotyl elongation assay

WT and mutant *Slbbx*20 seeds were surface sterilized with 30% (v/v) commercial bleach (2.7% w/v sodium hypochlorite) for 15 min with agitation, rinsed with distilled water, and inoculated in square culture vessels (16 vessels with 16 seeds each per genotype) containing sterile medium composed of 1/2× MS (Murashige and Skoog, 1962) and 2% (w/v) phytagel. The pH was adjusted to 5.7 ± 0.05. The seeds were kept in darkness for 4 d at 25 ± 2 °C to synchronize germination. After germination, on the fifth day, eight vessels per genotype were transferred to continuous white light [100 μmol m^{-2} s^{-1}, red/far-red (R/FR) 2.3], and eight were maintained under absolute darkness for another 4 d. On the eighth day, the length of the hypocotyls after light or dark treatment was measured, and five biological replicates of pooled hypocotyls/cotyledons were sampled for each treatment/genotype, frozen in liquid nitrogen, and stored at –80 °C for further analysis.

Reverse transcription and quantitative PCR analysis

RNA extraction, cDNA synthesis, and quantitative PCR (qPCR) assays were performed as described by Quadrana *et al*. (2013). Primer sequences and loci IDs are detailed in Supplementary Table S1. qPCRs were carried out in a QuantStudio 6 Flex Real-Time PCR system (Applied Biosystems) using 2× Power SYBR Green Master Mix reagent (Life Technologies) in a 10 μl final volume. Absolute fluorescence data were analyzed using the LinRegPCR software package (Ruijter *et al*., 2009) to obtain cycle quantitation (Cq) values and calculate PCR efficiency. Expression values were normalized against the geometric mean of two reference genes, *SlTIP41* and *SlEXPRESSED*, according to Quadrana *et al*. (2013). A permutation test lacking sample distribution assumption (Pfaffl *et al*., 2002) was applied to detect statistical differences (P≤0.05) in expression ratios using the algorithms in the fgStatistics software package (Di Rienzo, 2009).

Yeast two-hybrid assay

The complete coding sequence of *SlBBX20* (Solyc12g089240) was cloned into pGADT7 Gateway™ vector at the N-terminus of the activation domain (AD) of the GALACTOSIDASE 4 (GAL4) transcriptional activator. *SlHY5* (Solyc08g061130), *SlPIF4* (Solyc07g043580), and *SlRIN* (Solyc05g012020) interactors were cloned into pGBT9 Gateway™ vector at the N-terminus of the GAL4 DNA-binding domain (BD) (Cuéllar *et al*., 2013). *Saccharomyces cerevisiae* PJ69-4A strain (James *et al*., 1996) was co-transformed with both destination vectors using the polyethylene glycol (PEG)/lithium acetate method. Transformants were selected on SD (synthetic minimal) medium (Takara Bio, Shigo, Japan) lacking leucine and tryptophan. Three individual colonies were grown overnight in liquid cultures at 30 °C, and 10- or 100-fold dilutions were dropped on control (SD-Leu-Trp) and selective media (SD-Leu-Trp-His).

As SlBBX20 fused to the BD showed self-activation, all assays were conducted with this protein fused to the AD. For SlBBX20 and SlRIN interaction, the autoactivation inhibitor 3-aminotriazole (60 mM) was used.

Transient expression assay

For transient expression assays (TEAs), the coding sequences of *SlBBX20, SlPIF4*, *SlHY5*, and *SlRIN* were PCR-amplified from leaf cDNA with the primers listed in Supplementary Table S1 and cloned into pCR™ 8/GW/TOPO TA Cloning vector (Invitrogen). Subsequently, a Gateway LR II recombination reaction (Invitrogen) was performed with the p2GW7 vector (Vanden-Bossche *et al*., 2013), obtaining the effector constructs. The *SlBBX20* (977 bp), *SlPIF4* (1617 bp), *SlCHS1* (1170 bp), *SlCHI2* (1232 bp), *SlF3H* (926 bp), and *SlFLS* (1114 bp) promoter regions were PCR-amplified from leaf gDNA and cloned into pCR™ 8/GW/TOPO TA Cloning vector (Invitrogen). Next, Gateway LR II recombination reaction (Invitrogen) was performed with the pGWL7 vector (Vanden-Bossche *et al*., 2013), obtaining the promoter constructs harboring the *FIREFLY LUCIFERASE* (*fLUC*) reporter gene. TEAs were performed in protoplasts prepared from *N. tabacum* Bright Yellow-2 (BY-2) cells, as previously described Vanden-Bossche *et al.* (2013). Briefly, protoplasts were transfected with promoter/effector combinations. For normalization, a construct with the RENILLA (*rLUC*) reporter gene under the control of the cauliflower mosaic virus (CaMV) 35S promoter was co-transfected. As negative control, instead of an effector, a construct containing *pCaMV35S*::*GUS* was used. fLUC activity was expressed as the fLUC/rLUC activity ratio relative to the negative control.

Shade avoidance response assay

WT and mutant *Slbbx*20 seeds were sown in sowing trays with a 1:1 mixture of commercial substrate (Plantmax HT, Eucatex, Brazil) and vermiculite, maintained for 4 d in darkness for germination, kept for 2 d in constant white light for de-etiolation, and then submitted to white light (control)/shade treatment for 15 d. The white light treatment (WL) consisted of a combination of full spectrum, warm, and far-red LEDs with a neutral filter: PAR=40 μmol m^{-2} s^{-1}, red=7.6 μmol m^{-2} s^{-1}, blue=1.9 μmol m^{-2} s^{-1}, far-red=12.2 μmol m^{-2} s^{-1}. The shade light treatment was obtained with the same source of WL and a green acetate filter (#089; LEE Filters): PAR=40 μmol m^{-2} s^{-1}, red=4.0 μmol m^{-2} s^{-1}, blue=1.9 μmol m^{-2} s^{-1}, far-red=22.0 μmol m^{-2} s^{-1}. The R/FR ratios were 0.6 and 0.1 in WL and shade, respectively. Both treatments were performed at 25 ± 0.5 °C. Hypocotyl length was measured until reaching a plateau (maximum length, 6 d after white/shade light treatment). At the end of the treatment, the plant height and the first internode length were scored. Moreover, the mRNA level of the SAR inhibitor *PHYTOCHROME RAPIDLY REGULATED 1* (*SlPAR1*) was profiled in primordia (≤1 cm), young (≤2 cm) and expanding (≤3 cm) leaves.

Experimental planting and sampling for phenotypic characterization

For *Slbbx20* mutant phenotypic characterization, several experiments were carried out.

For vegetative growth evaluation, 20 plants per genotype were grown for 55 d. Total leaf number, leaf area, and dry weight were recorded. Total leaf area was obtained by digitizing all leaves and calculating the area in ImageJ software (Schneider *et al.*, 2012). Specific leaf area (SLA, cm^2 g^{-1}) was calculated as the ratio between leaf area and leaf dry weight. The fifth phytomer from bottom to top was collected for anatomical analysis.

For leaf development analysis, leaf primordia (≤1 cm), young (≤2 cm) and expanding (≤3 cm) leaves were sampled from seedlings 20 days after germination (DAG).

For floral meristem differentiation analysis, seeds were sown in vermiculite, left for 4 d in darkness to synchronize germination, and the apex meristem was dissected under a magnifying glass 4, 6, 8, 12, and 15 DAG. The meristems were classified according to their morphology. The corresponding cotyledons were pooled, frozen in liquid nitrogen, and stored at –80 °C for further analysis. Twenty-five seedlings were analyzed for each sampling point.

For flowering time, yield, and fruit quality analysis, two sets of 12 plants per genotype (destructive and non-destructive) were grown for 120 d. Flowering time was measured in both sets. The destructive set was used to sample fully expanded leaves (fifth phytomer from bottom to top) and fruit pericarp at mature green (MG; when the placenta displays a gelatinous aspect, ~33 d post-anthesis), breaker (Br; when the first signal of carotenoid accumulation is observed, ~36 d post-anthesis), and breaker+N (BrN; N days after breaker). Five biological replicates were sampled, each one composed of leaves or fruits from at least four plants. The non-destructive set was used for yield evaluation. The total number of flowers and fruits, total fresh weight (FW) of fruits, and vegetative aerial FW and dry weight (DW) were recorded. The harvest index (HI) was calculated according to the formula: HI=(total fruit FW)/(total vegetative aerial FW+total fruit FW).

Anatomical analysis

For leaf anatomical analysis, a fragment (1 × 0.5 cm) of the terminal leaflets from fully expanded leaves (fifth phytomer from bottom to top) was excised and fixed in FAA70 (formalin–acetic acid–ethanol 70%, 1:1:18) for 24 h under vacuum (500 mmHg). Subsequently, the samples were dehydrated in an ethanol series (10, 30, 70, 80, 90 and 95%, v/v) under vacuum (500 mmHg). Pre-infiltration was performed with resin and 95% ethanol (1:1) with daily 2 h under vacuum (500 mmHg) for 1 week, and infiltration was done in resin under the same conditions. Cross-sections of 5 μm thickness were mounted on blades and stained with 0.05% toluidine blue. The images were captured in a light microscope (Zeiss AxioScope A1, Jena, Germany) and analyzed in the ImageJ software (Schneider *et al.*, 2012).

3-Indoleacetic acid quantification

Endogenous indole-3-acetic acid (IAA) was extracted and quantified as described by Silveira *et al.* (2004). Briefly, 150 mg of powdered tissue was homogenized in 2.5 ml of the extraction buffer containing 80% (v/v) ethanol, 1% (w/v) polyvinylpyrrolidone-40, and 0.05 μCi of [^{3}H]IAA, used as an internal standard. Samples were incubated and subsequently centrifuged. The supernatant was collected and the extraction was repeated once. The combined supernatants were completely vacuum-dried, redissolved in 90 μl of 10% methanol/0.5% acetic acid, and filtered through a 0.2 μm membrane. IAA levels were determined by HPLC in a 5 μm C18 column (Shimadzu Shin-pack CLC ODS) with a fluorescence detector (excitation at 280 nm, emission at 350 nm). Fractions containing IAA were collected and analyzed in a scintillation counter (Packard Tri-Carb) to estimate losses during the procedure. IAA quantification was performed based on a standard curve.

Fruit colorimetric measurement

Fruit surface color was determined at the equator of each collected fruit using a colorimeter (Konica Minolta, CR-400, 8 mm aperture, D65 illuminant, USA). Three measurements were taken at the equator of each fruit, and average values were calculated as described in Cruz *et al.* (2018).

Extraction, identification, and quantification of carotenoids

Fruit carotenoid extraction was performed according to Sérino *et al.* (2009) with modifications. Aliquots of 200 mg FW of fruit samples were sequentially extracted with NaCl saturated solution and dichloromethane and hexane:diethyl ether (1:1 v/v). After centrifugation, the supernatant was collected, and the hexane:diethyl ether extraction was repeated three more times. All supernatants were combined, and samples were dried by vacuum and dissolved in 200 μl of acetonitrile. Chromatography was carried out on an HPLC-DAD (model: 1260 system, Agilent Technologies, USA) equipped with an autosampler using a Phenomenex Luna C18 column (250 × 4.6 mm; 5 μm particle diameter) at room temperature with a flow rate of 0.8 ml min^{-1} and injection volume of 20 μl. The chromatographic method was constituted by a gradient of mixtures of solvents A (ethyl acetate) and B (acetonitrile:water 9:1 v/v) of 0–4 min with 0–5% B; 4–12 min with 5–10% B; 12–17 min with 10–20% B; 17–20 min with 20–65% B; 20–35 min with 65% B; and 35–40 min with 65–0% B. Eluted compounds were detected between 340 nm and 700 nm, and quantified at 450 nm. Identification and quantification were determined with a calibration curve using commercial standards.

Extraction, identification, and quantification of phenolics

For phenolic content analysis, ~200 mg FW of fruit pericarp samples were extracted with 1 ml of 80% methanol (v:v) for 30 min in an ultrasonic bath at room temperature followed by collection of the supernatants by centrifugation (13 000 *g*, 4 min, 25 °C). Phenolic compounds were analyzed by the HPLC-DAD (model: 1260 system, Agilent Technologies, USA) equipped with an autosampler, using a Zorbax Eclipse Plus C18 column (150 × 4.6 mm, 3.5 μm particle diameter) at 45 °C with a flow rate of 1 ml min^{-1} and injection volume of 3 μl. The chromatographic method was constituted by a gradient of mixtures of solvents A (0.1 % acetic acid in water) and B (acetonitrile) of 0–6 min with 10% B; 6–7 min with 10–15% B; 7–22 min with 15% B; 22–23 min with 15–20% B; 23–33 min with 20% B; 33–34 min with 20–25% B; 34–44 min with 25% B; 44–54 min with 25–50% B; and 54–60 min with 50–100% B. Identification of metabolites was carried out through commercial or previously isolated components, and quantification was determined with a calibration curve using a commercial rutin standard.

Promoter analyses

For motif identification in *SlPIF4*, *SlBBX20*, *SlCHS1*, *SlCHI*, *SlF3H*, and *SlFLS* promoters, 2000 bp upstream the ATG start codon were retrieved from the Sol Genomics Network (https://solgenomics.net). Using the PlantPan 3.0 platform (Chow *et al.*, 2019), the following motifs were surveyed in the sequences: for BBXs, CCAAT (Ben-Naim *et al.*, 2006), CORE2 (TGTGN$_{2-3}$ATG, Tiwari *et al.*, 2010), CCACA (Gnesutta *et al.*, 2017), G-box (CACGTG, Song *et al.*, 2020) and modified G-box (TACGTG, Xiong *et al.*, 2019); for PIFs, PBE-box (CACATG, Zhang *et al.*, 2013), G-box (CACGTG, Toledo-Ortiz *et al.*, 2014) and E-box (CANNTG, Zhang *et al.*, 2013); for RIN, C[CT][AT][AT][AT][AT][AT][AT][AG]G (Bianchetti *et al.*, 2022) and modified CArG (C[ACT][AT][AT][AT][AT][AT][AT][ATG]G, Fujisawa *et al.*, 2013); and for HY5, ACE-box (ACGT, Wang *et al.*, 2021).

Extraction, identification, and quantification of glycoalkaloids

Fruit pericarps at Br10 from WT and *slbbx20* plants were harvested and snap-frozen in liquid nitrogen. Metabolite extraction was performed on 50 mg of powdered tissue using 1 ml of 80% methanol (v/v). Samples were centrifugated and the supernatant was vacuum-dried. The pellets were resuspended in 100 μl of MilliQ water. Samples were subjected to ultra performance liquid chromatography–high resolution MS (UPLC-HRMS) at the VIB Metabolomics Core Ghent. Aliquots of 10 μl were injected on a Waters Acquity UHPLC (Waters) device connected to a Vion HDMS Q-TOF mass spectrometer (Waters). Chromatographic separation was carried out on an ACQUITY UPLC BEH C18 (150 × 2.1 mm; 1.7 μm) column (Waters); column temperature was maintained at 40 °C. A gradient of two buffers was used for separation: buffer A (water+0.1% formic acid, pH 3) and buffer B (acetonitrile+0.1% formic acid, pH 3), as follows: 99% A decreased to 50% A in 30 min, decreased to 30% from 30 min to 35 min, and decreased to 0% from 35 min to 37 min. The flow rate was set to 0.35 ml min^{-1}. Electrospray ionization (ESI) was applied; the LockSpray ion source was operated in positive ionization mode under the following specific conditions: capillary voltage, 2.5 kV; reference capillary voltage, 2.5 kV; source temperature, 120 °C; desolvation gas temperature, 550 °C; desolvation gas flow, 800 l h^{-1}; and cone gas flow, 50 l h^{-1}. The collision energy for full MS scan was set at 4 eV for low energy settings; for high energy settings (HDMSe) it was ramped from 20 eV to 70 eV. For DDA-MSMS (data-dependent acquisition tandem MS), the low mass ramp was ramped between 15 eV and 50 eV, and the high mass ramp was ramped between 50 eV and 120 eV. Mass range was set from 50 Da to 1500 Da, and scan time was set at 0.1 s. Nitrogen (>99.5%) was employed as the desolvation and cone gas. Leucine-enkephalin (100 pg μl^{-1} solubilized in water:acetonitrile 1:1 v/v, with 0.1% formic acid) was used for the lock mass calibration, with scanning every 2 min at a scan time of 0.1 s. Profile data were recorded through a Unifi Workstation v2.0 (Waters). Data processing was performed with Progenesis QI software version 3.0 (Waters) for chromatogram alignment and compound ion detection. The detection limit was set at medium sensitivity with a minimum peak width of 0.03 min. Data are normalized to DW. In ESI+ ionization, 17475 compound ions were detected and aligned to a 'pooled sample'. Identification of steroidal glycoalkaloids (SGAs) was performed by analyzing a tomatine standard (Tomatine, #0602, Extrasynthese, France) and comparing the MS and MS/MS fragments.

Botrytis cinerea inoculation assay

Botrytis cinerea (strain B05) was grown and maintained on potato dextrose agar medium (1.5% agar, 2% potato extract, 2% dextrose). Conidia were collected from agar plates with distilled water and a glass rod, filtered, and resuspended in a 0.1 M sucrose/0.07 M KH_2PO_4 solution to induce germination (Elad, 1991).

Fruits at Br4 stage were inoculated as described by Cantu *et al.* (2009). Briefly, on the day of harvest, tomato fruits were disinfected by 10% (v/v) bleach followed by three water rinses. Fruits were punctured (2 mm depth, 1 mm diameter) at seven sites. Six sites were inoculated with 10 μl of conidial suspension (3000 spores μl^{-1}), and the seventh was inoculated with 10 μl of sterile water as control. Fruits were incubated for 2 d at 24 °C in a dark and damp environment. Lesion areas were measured on digital photographs using ImageJ software (Schneider *et al.*, 2012). Susceptibility was determined daily as disease incidence (percentage inoculation sites showing symptoms of tissue maceration or soft rot) and severity (diameters of the lesions). The evaluation of susceptibility was repeated three times with 15 fruits per replicate.

Data analyses

Differences in parameters were analyzed in Infostat software version 17/06/2015 (Di Rienzo *et al.*, 2011). When the dataset showed homoscedasticity, Student's *t*-test ($P \leq 0.05$) was performed to compare mutant plants against the control genotype. In the absence of homoscedasticity, a non-parametric comparison was performed by applying the Kruskal–Wallis test ($P \leq 0.05$). All values represent the mean of at least four biological replicates.

Results

SlBBX20 characterization and generation of a loss-of-function mutant

SlBBX20 (Solyc12g089240) encodes a protein of 329 amino acids with two B-box domains that belongs to the structure group IV of the BBX protein family (Lira *et al.*, 2020). The presence of nuclear localization signals (NLSs) was predicted with three different platforms. According to cNLS mapper, SlBBX20 protein has two non-classical bipartite NLSs at the N-terminal portion and one classical type 2 NLS at the C-terminal end, suggesting nuclear and cytoplasmic localization (Supplementary Fig. S2A). However, DeepLoc 2.0 and BaCelLo predicted SlBBX20 exclusively as a nuclear protein (Supplementary Table S2). This result was validated by fusing the *SlBBX20* coding sequence to GFP. The transient expression of the fusion protein in *N. benthamiana* leaves confirmed that SlBBX20 is indeed targeted to the nucleus (Supplementary Fig. S2B). Additionally, SlBBX20 homodimerization was confirmed by BiFC assay (Supplementary Fig. S2B).

To further investigate SlBBX20 function, a knockout mutant line was obtained by CRISPR/Cas9-mediated genome

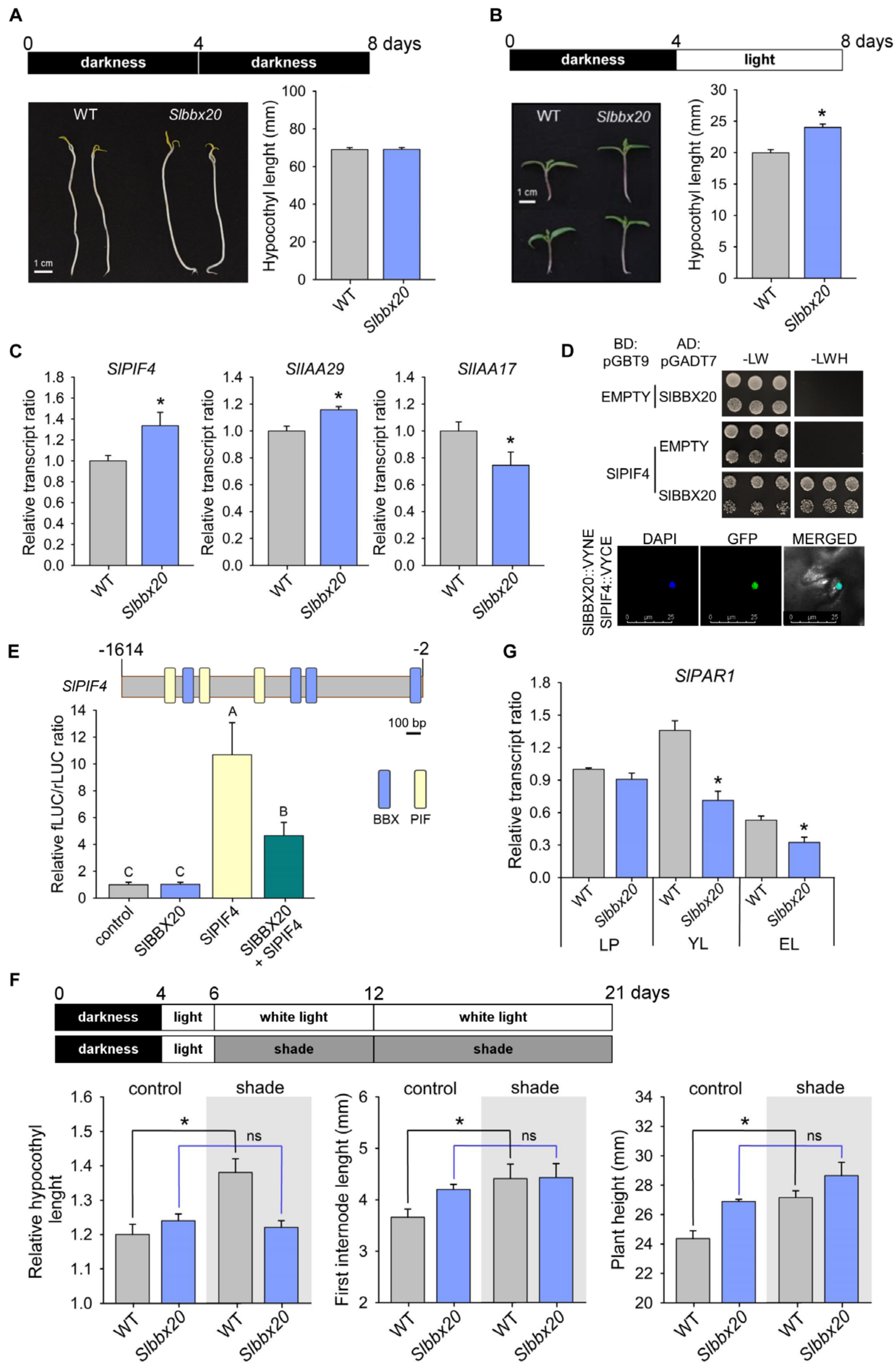

Fig. 1. *Slbbx20* seedlings are hyposensitive to light. (A and B) WT and *Slbbx20* seeds were sown *in vitro*, maintained for 4 d in darkness for germination, and then kept for an additional 4 d in constant white light or darkness. (A) Phenotype of seedlings after dark treatment. Values are means ±SE (n=120). (B) Phenotype of seedlings after light treatment. Values are means ±SE (n=120). Asterisks indicate a statistically significant difference from the

corresponding WT control ($P \leq 0.05$). (C) Histograms show the relative expression of *PHYTOCHROME INTERACTING FACTOR 4* (*SlPIF4*) and *AUXIN/INDOLE-3-ACETIC ACID29* (*SlIAA29*) and *SlIAA17* signaling genes in seedling hypocotyls after light treatment. Values are means ± SE of at least three biological replicates relative to the respective WT control. Asterisks indicate a statistically significant difference from the corresponding WT control ($P \leq 0.05$). (D) Yeast two-hybrid interactions between SlBBX20 and SlPIF4. SlBBX20 was fused to the activation domain and SlPIF4 to the binding domain. EMPTY, autoactivation control; -LW, positive control in non-selective medium without leucine and tryptophan; -LWH, selective medium without leucine, tryptophan, and histidine. Black boxes show three individual colonies at 10- and 100-fold dilutions. Ther panel below shows heterodimerization of SlBBX20 and SlPIF4 proteins by BiFC. SlBBX20::VYNE/SlPIF4::VYCE fusion proteins were transiently expressed in *Nicotiana benthamiana* leaves by infiltration with *Agrobacterium tumefaciens*. DAPI, nuclear marker, GFP, bright-field merged signals are indicated above the panels. (E) BBX and PIF transcription factor motifs identified in the *SlPIF4* gene promoter. BBX: CCAAT (Ben-Naim *et al*., 2006), CCACA (Gnesutta *et al*., 2017); and PIF: E-box (CANNTG, Zhang *et al.*, 2013). Numbers indicate nucleotide positions upstream of the ATG. Transactivation assay in *Nicotiana tabacum* BY-2 protoplast cells of the *SlPIF4* promoter by SlBBX20 and SlPIF4. Luciferase activity is expressed as the LUCIFERASE/RENILLA activity ratio relative to the negative control. Values are means ± SE (n=8). Different letters indicate significant differences ($P \leq 0.05$). (F) Shade avoidance response of *Slbbx20* seedlings. The relative hypocotyl length is expressed as the ratio between the maximum value obtained after 6 d of white light/shade treatment and the respective value at the beginning of the treatment. Internode length and plant height were measured after 15 d of shade treatment. Values are means ±SE (n=12). Asterisks indicate a statistically significant difference from the corresponding WT control ($P \leq 0.05$). ns: non-significant. (G) Relative expression of *PHYTOCHROME RAPIDLY REGULATED1* (*SlPAR1*) during leaf development stages: leaf primordia (LP), young (YL) and expanding leaves (EL) of WT and *Slbbx20*. Values are means ±SE of at least three biological replicates relative to the respective WT control. Asterisks indicate a statistically significant difference from the corresponding WT control ($P \leq 0.05$).

editing using two target guides (Supplementary Fig. S3A). the *Slbbx20* mutant harbors a deletion of 967 bp and an insertion of 14 bp, generating a premature stop codon that results in a truncated protein of 28 amino acids without any recognizable domain (Supplementary Fig. S3A). The *SlBBX20* mRNA in the mutant was almost undetectable (Supplementary Fig. S3B), most probably due to mRNA nonsense-mediated decay triggered by the premature termination codon in the expressed transcript (Lykke-Andersen and Bennett, 2014).

SlBBX20 regulates seedling photomorphogenesis and shade avoidance response

As the canonical function of BBX proteins is associated with seedling photomorphogenesis, an experiment was performed to investigate *Slbbx20* seedling development under different light conditions. After 4 d of dark treatment, mutant hypocotyls showed no difference in length compared with WT counterparts (Fig. 1A). However, mutant seedlings had longer hypocotyls when maintained under constant white light (Fig. 1B). In *A. thaliana*, increased hypocotyl growth under prolonged shade depends on *PIF4*-mediated auxin signaling, but does not rely on maintaining elevated auxin biosynthetic rates in the cotyledon (Pucciariello *et al*., 2018). In fact, the expression of the auxin biosynthetic genes reduces after several hours of exposure to low R/FR ratios (de Wit *et al*., 2015). Persistent PIF4 activity is needed for hypocotyl elongation under prolonged shade because it induces *INDOLE-3-ACETIC ACID 19* (*IAA19*) and *IAA29* auxin signaling factors, which are repressors of *IAA17*, a major inhibitor of hypocotyl growth (Pucciariello *et al*., 2018). In this context, to understand the mechanism underlying the observed phenotype, we examined auxin content by monitoring the mRNA levels of the biosynthetic genes in cotyledons. As observed in *A. thaliana*, the mRNA levels of the five tested genes did not indicate that altered auxin biosynthesis is responsible for the higher hypocotyl elongation observed in the *Slbbx20* mutant (Supplementary Fig. S4). In contrast, analysis of *SlPIF4*-mediated auxin signaling in hypocotyl revealed the up-regulation of *SlPIF4* and *SlIAA29*, while *SlIAA17* was down-regulated in *Slbbx20* (Fig. 1C). To better understand the role of SlBBX20 in this transcriptional cascade, we first demonstrated the physical interaction between SlBBX20 and SlPIF4 by Y2H and BiFC assays (Fig. 1D). In addition, TEAs revealed that SlPIF4 induces its own promoter, while the presence of SlBBX20 diminishes this transcriptional activation (Fig. 1E). This agrees with what is observed in *A. thaliana* where AtPIF4 binds its own promoter, inducing its transcriptional activity (Lee *et al*., 2021). Altogether, these results indicate that SlBBX20 is a positive regulator of photomorphogenesis and participates in light-mediated hypocotyl elongation inhibition through the negative control of SlPIF4 activity via heterodimerization.

To further investigate the light signaling impairment observed in the *Slbbx20* mutant, we analyzed the shade avoidance response (SAR) by exposing the tomato plants for 15 d under a low R/FR ratio (Fig. 1F). As evidenced by the increased hypocotyl and first internode length, and plant height, WT plants triggered SAR after low R/FR ratio treatment. In contrast, the *Slbbx20* mutant phenotype was similar to that observed for WT plants maintained in shade conditions regardless of the light treatment. In line with this phenotype, the expression of the negative regulator of SAR, *SlPAR1*, was diminished in mutant leaves (Fig. 1G). Hence, these findings implicate SlBBX20 as a negative regulator of SAR in tomato.

SlBBX20 positively regulates vegetative growth

The functional characterization of *SlBBX* genes, particularly *SlBBX17* and *SlBBX28*, identified these genes as regulators of vegetative growth (Lira *et al*., 2022; Xu *et al*., 2022). To address whether this is also the case for *SlBBX20*, the development of 55-day-old *Slbbx20* plants was examined by measuring biomass parameters. Mutant plants were shorter with reduced leaf number and area, resulting in diminished DW (Fig. 2A). Interestingly, the SLA was higher in *Slbbx20* than in WT plants (Fig. 2A). To further dissect this phenotype, a morpho-anatomical analysis was performed. The mutant leaf lamina was thinner due to the reduced thickness of the adaxial epidermis and the palisade and spongy parenchyma without changes in the number of cell layers (Fig. 2B). However, in *Slbbx20* mutant leaves, the number of palisade parenchyma cells per length unit was higher than in WT counterparts (Fig. 2B).

The mechanism underlying the observed misregulation of cell division and/or expansion was investigated through a comprehensive transcriptional profile during leaf development (Fig. 2C; Supplementary Table S3). Auxins play a central role in controlling cell division and expansion (Perrot-Rechenmann, 2010; Gomes and Scortecci, 2021); therefore, its metabolism was investigated. In *Slbbx20* leaf primordia, the expression of auxin biosynthetic genes, namely *TRYPTOPHAN AMINOTRANSFERASE 1* (*SlTAR1*) and two *YUCCA-LIKE FLAVIN MONOOXYGENASES* (*SlYUC1* and *SlYUC2*), was up-regulated, in line with the observed increment in auxin content. Accordingly, cell division-related genes, namely *CYCLIN-DEPENDENT KINASE-B2* (*SlCDKB2*) and three *CYCLIN* genes (*SlCYCB1*, *SlCYCB2*, and *SlCYCD3*), were also induced in the *Slbbx20* mutant (Fig. 2C; Supplementary Table S3). In contrast, *EXPANSIN-A5* (*SlEXPA5*), the most abundant *SlEXP* expressed in leaves according to TomExpress (Zouine *et al.*, 2017), was down-regulated in young and expanding *Slbbx20* leaves.

Collectively, these data indicate that SlBBX20 regulates auxin metabolism, ensuring the proper cell division and expansion rate, and playing a positive role in controlling vegetative growth.

Loss of *SlBBX20* disturbs flowering and yield

Flowering has been known to be regulated by BBX proteins since the first functional characterization of a member of this family. AtBBX1, also known as CONSTANS (AtCO; Putterill *et al.*, 1995), is an inducer of the florigen *FLOWERING LOCUS T* (*AtFT*). Once synthesized in leaves, AtFT protein is translocated to the shoot apex, where it induces meristem transition from vegetative to floral (An *et al.*, 2004). Hitherto, several other BBXs have been identified as positive or negative regulators of flowering (Cao *et al.*, 2023). Thus, we examined whether SlBBX20 plays a role in tomato flowering. *Slbbx20* plants delayed the first anthesis without increasing the number of leaves (Fig. 3A). Then, we monitored the meristem transition in WT and *Slbbx20* seedlings (Fig. 3B). Both genotypes had the apical meristem still in the vegetative stage at 4 DAG. While the meristem transition began 6 DAG in WT seedlings, this only occurred 8 DAG in *Slbbx20* seedlings. Even 15 DAG, when all WT meristems were in either the transition or floral stage, some *Slbbx20* meristems were still vegetative. The transcriptional profile of *SlSFT* in the cotyledons explained this delay since its transcript peak shifted from 4 DAG in WT to 8 DAG in *Slbbx20* seedlings (Fig. 3C).

Given the developmental delay observed, we investigated the effect of SlBBX20 deficiency on plant yield. After cultivation for 120 d, the number of flowers produced by the mutant was 50% lower than in WT plants, resulting in fewer fruits per plant (Fig. 3D). Ultimately, as both total fruit and shoot weight were reduced, the harvest index of the *Slbbx20* plants did not differ from that of the WT genotype (Fig. 3D). These results suggest that mutant plants have a general delay in development rather than a direct regulation of flowering time.

Altogether, the data presented unveil SlBBX20 as a pivotal factor in vegetative and reproductive development.

SlBBX20 expression is induced by the fruit ripening regulator SlRIN

SlBBX20 mRNA levels have been shown to increase during fruit ripening (Supplementary Fig. S1), and SlRIN, a master ripening regulator TF, binds to the *SlBBX20* promoter (Lira *et al.*, 2020), suggesting that SlRIN induces *SlBBX20* transcription. To further investigate this relationship, *SlBBX20* transcripts were profiled in *Slrin* mutant fruits. At the MG stage, no differences were detected between genotypes. With the onset of ripening, the amount of *SlBBX20* transcript rapidly accumulated from the MG to Br stage, remaining constant until the fully ripe stage (Br10) in WT fruits. However, *Slrin* mutant fruits displayed reduced levels of *SlBBX20* mRNA compared with their WT counterparts (Fig. 4A). In contrast, *SlRIN* transcripts were unaltered in *Slbbx20* fruits (Supplementary Fig. S5).

BBX (Cao *et al.*, 2023) and SlRIN TFs (Bemer *et al.*, 2012) are known to heterodimerize with other regulatory factors; thus, the putative interaction between SlBBX20 and SlRIN was tested and confirmed by BiFC and Y2H assays (Fig. 4B). Additionally, not only does SlRIN bind to the *SlBBX20* promoter (Lira *et al.* 2020), but putative BBX-binding motifs were also found in the promoter of *SlBBX20*. Therefore, we performed a TEA to better understand the ripening-related transcriptional regulation of this gene and the biological significance of SlRIN–SlBBX20 interaction (Fig. 4C). Either SlRIN or SlBBX20 alone induced the *SlBBX20* gene promoter by ~30% of the basal activity. Interestingly, the presence of both TFs together resulted in an overinduction of the *SlBBX20* promoter, increasing the fLUC/rLUC ratio to 170%. These results unveiled that *SlBBX20* ripening-associated expression is triggered by the combined activity of SlRIN and SlBBX20.

SlBBX20 positively regulates fruit flavonoid accumulation

Ripe fruits of the *Slbbx20* mutant displayed a visible orangish color, which was confirmed by a higher Hue angle compared with its WT counterparts (Supplementary Fig. S6). In tomato,

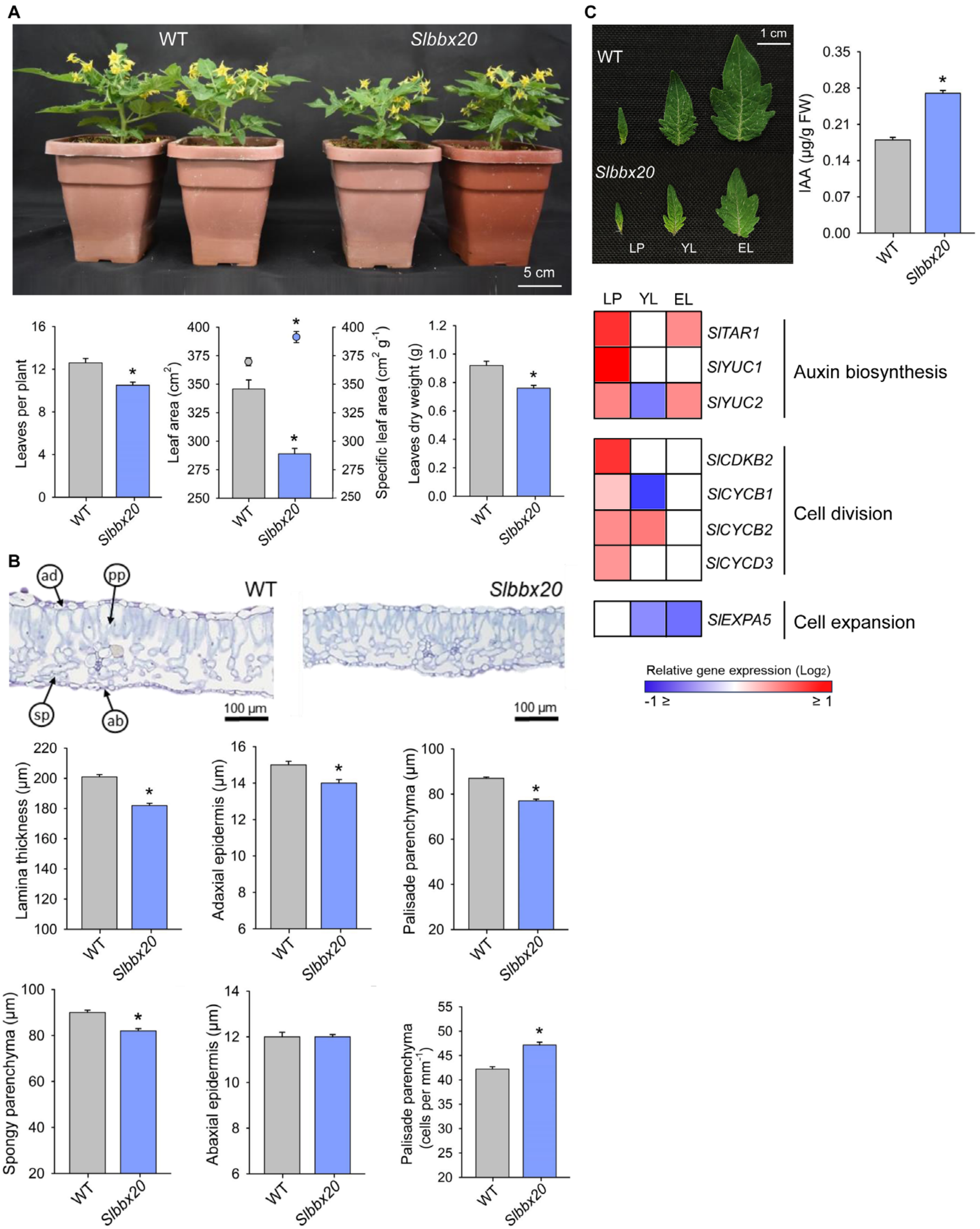

Fig. 2. SlBBX20 positively controls vegetative growth. (A) WT and *Slbbx20* plants cultivated for 55 d, number of leaves, total (bars) and specific (dots) leaf area, and leaf DW. Values are means ±SE (*n*=15). Asterisks indicate a statistically significant difference from the WT control (*P*≤0.05). (B) Leaf cross-sections and tissue anatomy. ad, adaxial epidermis; pp, palisade parenchyma; sp, spongy parenchyma; ab, abaxial epidermis. The histograms

show lamina thickness measurements and the number of layers of palisade parenchyma. Values are means ±SE (*n*=7). Asterisks indicate a statistically significant difference from the WT control (*P*≤0.05). (C) Leaf development stages: leaf primordia (LP), young (YL) and expanding leaves (EL) of WT and *Slbbx20*. Auxin (indole-3-acetic acid, IAA) content in leaf primordia. Values are means ±SE (*n*=4). Asterisks indicate a statistically significant difference from the WT control (*P*≤0.05). Heatmaps indicate statistically significant differences in mRNA (*n*=4) content in *Slbbx20* leaves relative to the respective WT sample (*P*≤0.05). The absolute relative transcript values are detailed in Supplementary Table S3. Abbreviations: *TRYPTOPHAN AMINOTRANSFERASE-1* (*SlTAR1*), *YUCCA-LIKE FLAVIN MONOOXYGENASE-1* (*SlYUC1* and *SlYUC2*), *CYCLIN-DEPENDENT KINASE-B2* (*SlCDKB2*), *CYCLIN-B1* (*SlCYCB1*; *SlCYCB2* and *SlCYCD3*), *EXPANSIN-A5* (*SlEXPA5*) during leaf development.

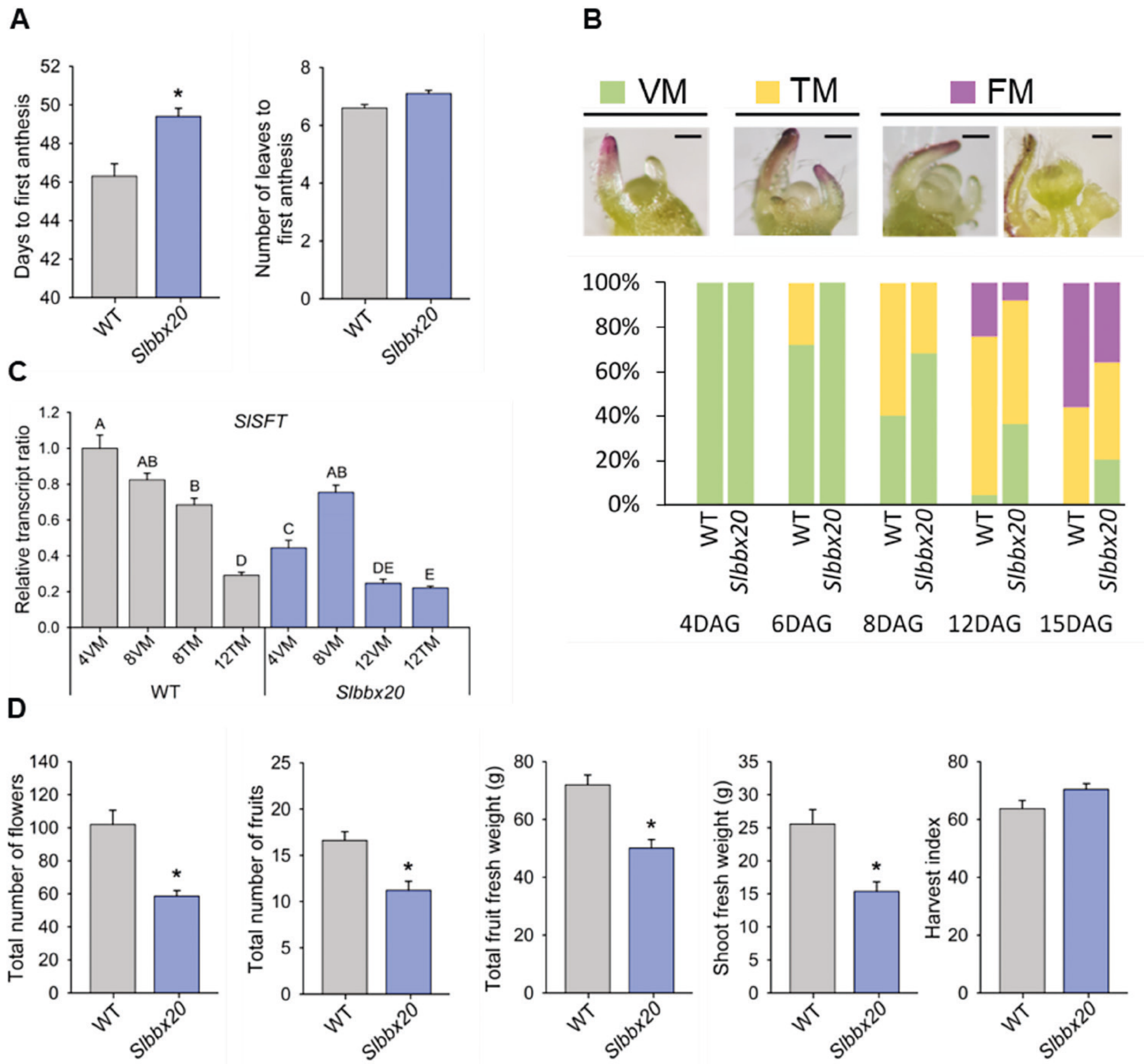

Fig. 3. SlBBX20 regulates flowering and yield. (A) Days and number of leaves until the first anthesis. Values are means ±SE (*n*=15). Asterisks indicate a statistically significant difference from the WT control (*P*≤0.05). (B) The meristem from 4, 6, 8, 12, and 15 DAG; seedlings were classified as vegetative (VM), transition (TM), and floral (FM). Scale bar=100 μm. *n*=25. (C) Relative expression of the florigen *SINGLE FLOWER TRUSS* (*SlSFT*) in cotyledons of 4, 8, or 12 DAG seedlings with VMs or TMs. Values are means ±SE of at least three biological replicates relative to the WT 4VM sample. Different letters indicate statistically significant differences (*P*≤0.05). (D) Yield parameters in 120-day-old plants. Values are means ±SE (*n*=15). Asterisks indicate a statistically significant difference from the WT control (*P*≤0.05).

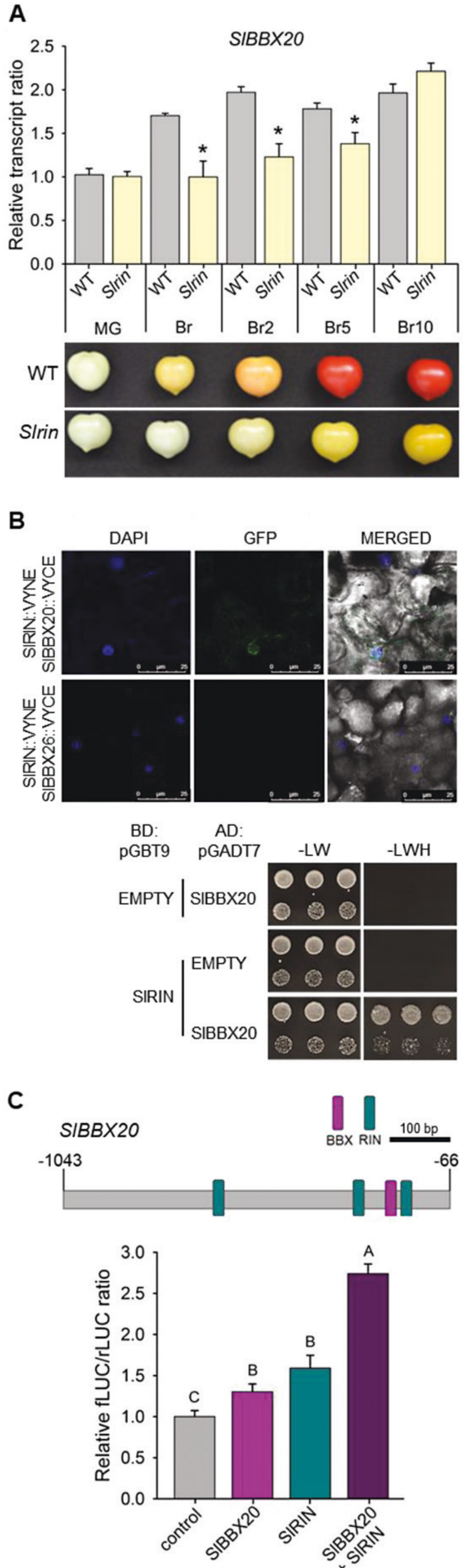

Fig. 4. SlRIN induces *SlBBX20* expression during ripening. (A) Relative expression of *SlBBX20* in fruits from the *Slrin* mutant. The bottom panel shows the corresponding phenotype of WT and *Slrin* fruits. Values are means ±SE of at least three biological replicates relative to the WT MG sample. Asterisks indicate a statistically significant difference from the corresponding WT control ($P \leq 0.05$). (B) Heterodimerization of SlBBX20 and SlRIN proteins. SlRIN::VYNE/SlBBX20::VYCE and SlRIN::VYNE/SlBBX26::VYCE fusion proteins were transiently expressed in *Nicotiana benthamiana* leaves by infiltration with *Agrobacterium tumefaciens*. SlBBX26 was used as interaction negative control. DAPI, nuclear marker; GFP, bright-field merged signals are indicated above the panels. The panel below shows yeast two-hybrid interactions between SlBBX20 and SlRIN. SlBBX20 was fused to the activation domain and SlRIN to the binding domain. EMPTY, autoactivation control; -LW, positive control in non-selective medium without leucine and tryptophan; -LWH, selective medium without leucine, tryptophan, and histidine. Black boxes show three individual colonies at 10- and 100-fold dilutions. (C) RIN and BBX transcription factor motifs identified in the *SlBBX20* gene promoter. RIN: C[CT][AT][AT][AT][AT][AT][AT][AG]G (Bianchetti *et al*., 2022), modified CArG (C[ACT][AT][AT][AT][AT][AT][AT][ATG]G, Fujisawa *et al*., 2013); and BBX: CCAAT (Ben-Naim *et al*., 2006), CORE2 (TGTGN2-3ATG, Tiwari *et al*., 2010), CCACA (Gnesutta *et al*., 2017), G-box (CACGTG, Song *et al*., 2020), modified G-box (TACGTG, Xiong *et al*., 2019). Numbers indicate nucleotide positions upstream of the ATG. The histogram shows the transactivation assay in *Nicotiana tabacum* BY-2 protoplast cells of the *SlBBX20* promoter by SlBBX20 and SlRIN. Luciferase activity is expressed as the LUCIFERASE/RENILLA activity ratio relative to the negative control. Values are means ±SE (n=8). Different letters indicate significant differences ($P \leq 0.05$).

two classes of specialized metabolites are responsible for fruit pigmentation, carotenoids and flavonoids (Dhar *et al*., 2015). Surprisingly, only some punctate differences in phytoene and phytofluene, which are colorless carotenoids, were detected in *Slbbx20* fruits, without altering the total carotenoid content (Supplementary Table S4). In contrast, the three classes of flavonoids (i.e. naringenin chalcone, kaempferol, and quercetin derivatives) were dramatically reduced in mutant fruits, especially at the fully ripe stage (Br10, Fig. 5; Supplementary Table S5).

To understand how SlBBX20 regulates flavonoid accumulation, we profiled the mRNA amount of the following biosynthetic genes: *CHALCONE SYNTHASE* (*SlCHS1* and 2), *CHALCONE ISOMERASE* (*SlCHI*), *FLAVANONE 3-HYDROXYLASE* (*SlF3H*), *FLAVANONE 3'-HYDROXYLASE* (*SlF3'H*), and *FLAVONOL SYNTHASE* (*SlFLS*). In the case of *SlCHI* that has six paralogs, the only one expressed in fruits according to TomExpress (Zouine *et al*., 2017) was selected. In line with the flavonoid content, with the exception of *SlCHS2* that was unaltered (Supplementary Table S6), the tested genes were strongly down-regulated during the ripening of mutant fruits (Fig. 5).

In tomato seedlings, the expression of flavonoid biosynthetic genes was induced by SlBBX25 overexpression, leading to anthocyanin accumulation (Luo *et al*., 2021). Moreover, the lack of SlHY5 resulted in the reduction of fruit flavonoid content, as well as the down-regulation of the corresponding biosynthetic genes and *SlBBX20* mRNA levels (Wang *et al*., 2021). In this context, our results led to the hypothesis that SlBBX20 plays a role in SlHY5-mediated flavonoid induction. Interestingly, the physical interaction between SlBBX20 and SlHY5 was previously reported by Yang *et al*. (2022) and confirmed here by Y2H assay (Fig. 6A). Furthermore, the transcriptional induction

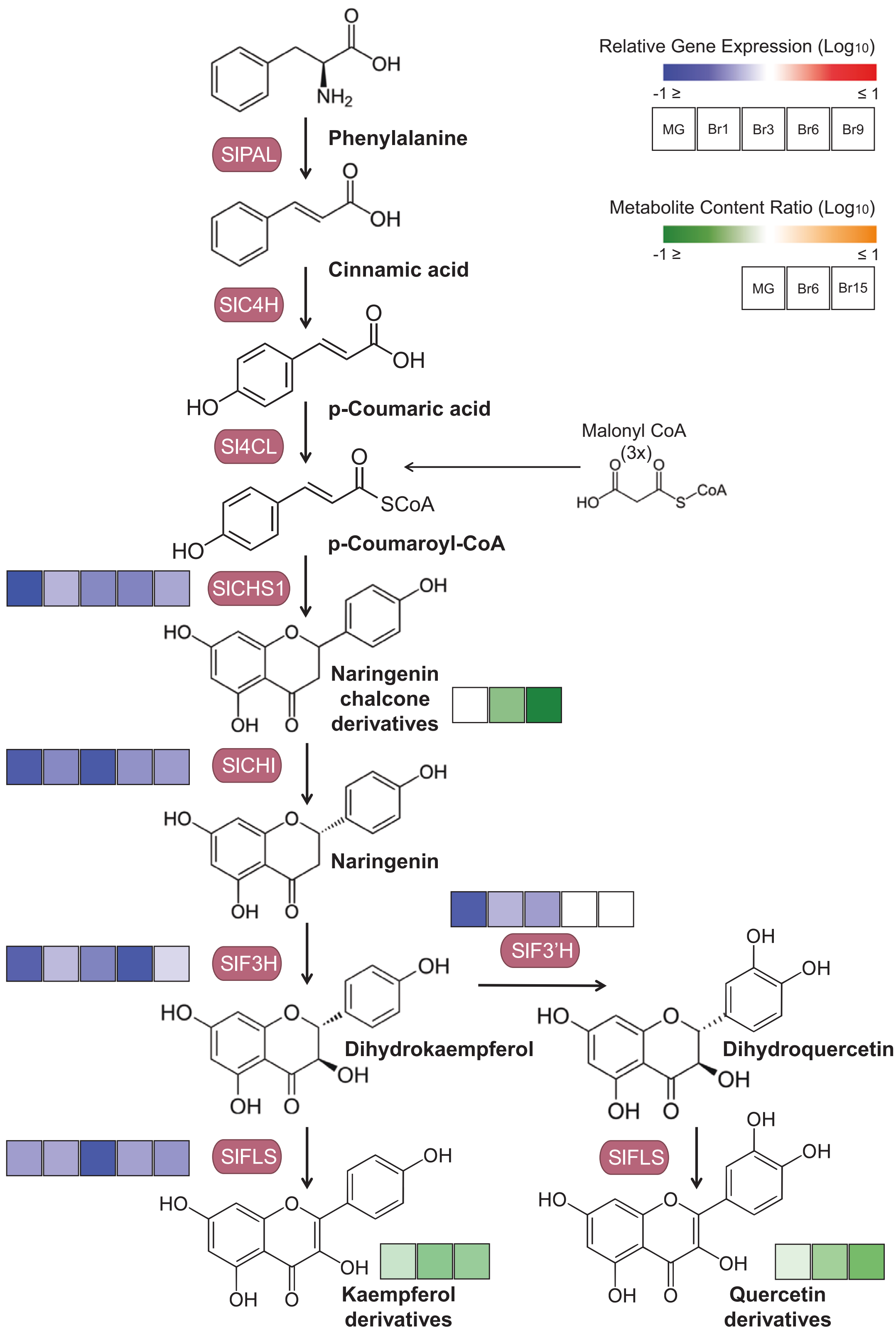

Fig. 5. SlBBX20 promotes fruit flavonoid biosynthesis. Flavonoid biosynthetic pathway. Heatmaps indicate statistically significant differences in metabolites (*n*=4) and mRNA (*n*=3) content in *Slbbx20* fruits relative to the respective WT sample ($P \le 0.05$). The absolute metabolite and relative transcript values are detailed in Supplementary Table S5 and S6. Abbreviations: PHENYLALANINE AMMONIA-LYASE (SlPAL), CINNAMATE 4 HYDROXYLASE (SlC4H), 4-COUMARATE-CoA LIGASE (SlC4L), CHALCONE SYNTHASE 1 (SlCHS1), CHALCONE ISOMERASE (SlCHI), FLAVANONE 3-HYDROXYLASE (SlF3H), FLAVANONE 3'-HYDROXYLASE (SlF3'H), and FLAVONOL SYNTHASE (SlFLS). Created with BioRender.com.

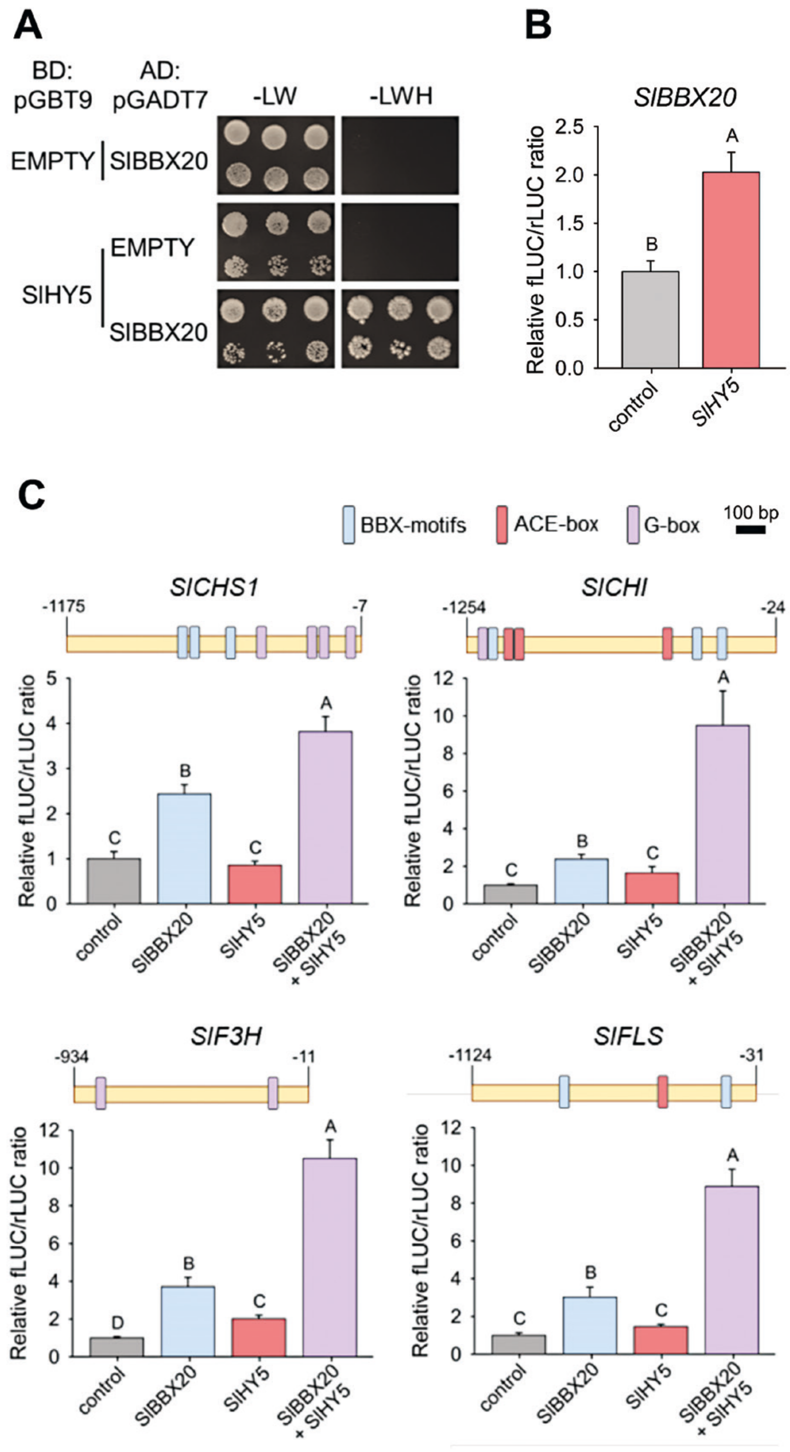

Fig. 6. SlBBX20 induces the transcriptional activity of flavonoid biosynthetic genes. (A) Yeast two-hybrid interactions between SlBBX20 and SlHY5. SlBBX20 was fused to the activation domain and SlHY5 to the binding domain. EMPTY, the same autoactivation control as in Fig. 1D; -LW, positive control in non-selective medium without leucine and tryptophan; -LWH, selective medium without leucine, tryptophan, and histidine. Black boxes show three individual colony cultures at 10- and 100-fold dilutions. (B) Transactivation assay in *Nicotiana tabacum* BY-2 protoplast cells of the *SlBBX20* promoter by SlHY5. Luciferase activity is expressed as the LUCIFERASE/RENILLA activity ratio relative to the negative control. Values are means ±SE (*n*=8). Different letters indicate significant differences (*P*≤0.05). (C) BBX- and HY5-binding motifs in flavonoid biosynthetic gene promoters (yellow lines) are shown. BBX motifs: CCAAT (Ben-Naim *et al*., 2006), CORE2 (TGTGN$_{2-3}$ATG, Tiwari *et al*., 2010), CCACA (Gnesutta *et al*., 2017). HY5 motif: ACE-box (ACGT, Wang *et al*., 2021). Common motifs: G-box (CACGTG, Song *et al*., 2020) and modified G-box (TACGTG, Xiong *et al*., 2019). Numbers indicate nucleotide positions upstream of the ATG. Histograms show the transactivation assay in *Nicotiana tabacum* BY-2 protoplast cells of flavonoid biosynthetic gene promoters by SlBBX20 and/or SlHY5 as effectors. Luciferase activity is expressed as the LUCIFERASE/RENILLA activity ratio relative to the negative control. Values are means ±SE (*n*=8). Different letters indicate significant differences (*P*≤0.05).

of *SlBBX20* by SlHY5 was demonstrated by TEA (Fig. 6B). Through an *in silico* analysis, putative binding motifs for both these proteins were found in the promoter of *SlCHS1*, *SlCHI*, *SlF3H*, and *SlFLS*. Then, a TEA was performed with SlBBX20 and/or SlHY5 as effectors (Fig. 6C). While SlBBX20 activated up to four times the tested promoters and SlHY5 had little to no effect on their transcriptional activity, the presence of both effectors dramatically induced the basal fLUC/rLUC ratio up to 10 times.

These results indicated that SlBBX20 induces flavonoid accumulation in fruits by up-regulating the transcription of the biosynthetic genes through the heterodimerization with SlHY5.

Loss of *SlBBX20* decreases the accumulation of steroidal glycoalkaloids in tomato fruit

It has been previously shown that SlHY5 also regulates SGA production in tomato, by directly binding to biosynthetic gene promoters (Wang *et al.*, 2018). Based on this information and the interaction between SlHY5 and SlBBX20, demonstrated above, we investigated whether SGA accumulation is affected in fully ripe (Br10) fruits by loss of SlBBX20. To this end, we performed targeted metabolomics in fully ripe tomato fruit from WT and mutant plants. We observed a decrease in the levels of α-tomatine and dehydrotomatine, as well as in SGAs downstream of α-tomatine (i.e. putative acetoxytomatine, hydroxytomatine, and esculeoside) (Supplementary Table S7).

SlBBX20 attenuates *Botrytis cinerea* infection

Common factors between light and defense signaling transduction pathways have been reported (Pierik and Ballaré, 2021). Moreover, flavonoids are important nutraceutical compounds with antioxidant activity that play a major role in post-harvest disease resistance (Hoensch and Oertel, 2015). Indeed, high concentrations of these compounds in fruits often correlate with a low incidence of pathogens (Treutter, 2006). Tomatine also plays an important role in biotic defense, and the ability of the pathogen to deactivate this compound determines the success of infection (Sandrok and VanEtten, 1998; Ito *et al.*, 2007; Pareja-Jaime *et al.*, 2008; Dahlin *et al.*, 2017). Due to the above-demonstrated effect of SlBBX20 on flavonoid and SGA accumulation, *Slbbx20* fully ripe fruits were inoculated with the necrotrophic fungus *B. cinerea*. The number of infected inoculated sites and the lesion area were higher in *Slbbx20* than in WT fruits 48 h post-infection (Fig. 7).

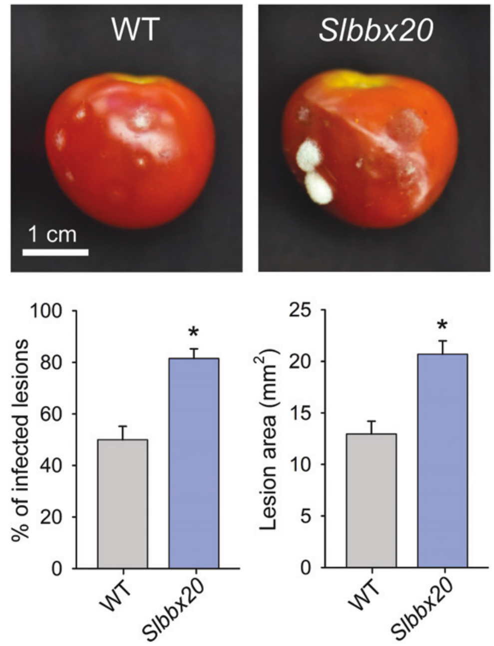

Fig. 7. SlBBX20 participates in the defense response. Representative WT and *Slbbx20* fruits at the Br10 stage 48 h after infection with *Botrytis cinerea.* The fruits were punctured and inoculated with fungal conidia. Histograms show disease incidence and severity. Values are means ±SE (n=15). Asterisks indicate a statistically significant difference from the WT control ($P \leq 0.05$).

Discussion

Knowledge of the *BBX* gene family has greatly increased in recent years, revealing BBX proteins as regulatory factors that play pleiotropic roles in plant growth (Cao *et al.*, 2023). Consequently, their study in crop species is particularly interesting since by affecting different stages of plant development, BBXs can modulate agronomically important traits, such as the yield and quality of harvestable organs (Shalmani *et al.*, 2023). In this sense, here, we functionally characterized tomato *SlBBX20* (Solyc12g089240), which encodes a BBX protein with two B-box domains and whose transcription is abruptly up-regulated upon fruit ripening in a phytochrome-mediated manner (Lira *et al.*, 2020).

The behavior of the *Slbbx20* mutant in response to distinct growth conditions demonstrated that SlBBX20 is a positive regulator of light signaling, reinforcing its previously described role as a downstream factor in the phytochrome-mediated signaling cascade (Lira *et al.*, 2020). Our data showed that SlBBX20 participates in light-mediated growth inhibition through the heterodimerization with SlPIF4 (Fig. 1) that, in turn, negatively regulates SlPIF4 activity and, consequently, the downstream auxin signaling cascade (i.e. *SlIAA29* and *SlIAA17*). In the absence of SlBBX20, mutant plants are hyposensitive to light, maintaining higher PIF4-mediated crosstalk between light and auxin signaling, as observed in *A. thaliana* under prolonged shade (Pucciariello *et al.*, 2018). In agreement with this regulatory mechanism, the physical interaction between AtPIF4 and AtBBX11 inhibits AtPIF4-mediated *AtIAA29* transcriptional induction (Song *et al.*, 2021).

Plants have two strategies to deal with shade: shade tolerance and shade avoidance. Shade-tolerant species are adapted to the understorey of tree canopies (Gommers *et al.*, 2013). In contrast, shade avoidance is induced by a low PAR and a low R/FR ratio, and, in this case, plants maximize light capture by increasing stem length and positioning the leaves out of the shade via photoreceptor signaling networks (Fernández-Milmanda and Ballaré, 2021). Several reports have investigated the effect of prolonged shade on the growth and phenology of shade-avoiding plants. *A. thaliana* plants grown under constant shade developed fewer leaves with reduced area due to an attenuated leaf initiation and cell expansion rate, respectively (Cookson and Granier, 2006). Further experiments showed that while energy signals mediated by TARGET OF RAPAMYCIN kinase pathway are sufficient to stimulate cell proliferation in the shoot meristem even in the dark, the development of a normal leaf lamina requires photomorphogenesis-like hormonal responses (Mohammed *et al.*, 2018). Similar results have been observed in soybean, as plants grown under shade conditions showed decreased leaf size caused by the differential expression of cell proliferation and/or expansion genes dependent on the leaf developmental stage (Wu *et al.*, 2017). Similarly, *Slbbx20* plants displayed a misregulation of these processes (Fig. 2). Although mutant leaves contained more cells due to an increased expression of cell division-related genes preceded by a peak in auxin biosynthesis at the leaf primordia stage, cell size was compromised by the reduced amount of *SlEXPA5* mRNA in expanding leaves, resulting in plants with diminished size. Shade also delays flowering and compromises yield in strawberry (Takeda *et al.*, 2010) and soybean (Cober and Voldeng, 2001; Kurosaki and Yumoto, 2003), as observed in the *Slbbx20* mutant (Fig. 3). In conclusion, SlBBX20 deficiency phenocopies plants growing under shade conditions displaying a seemingly constitutive SAR, which delays vegetative and reproductive growth resulting in smaller plants with reduced yield.

Recent reports have shown a key role for BBX proteins as inducers of specialized metabolism in tomato fruits. SlBBX25 (Solyc01g110180) is a positive regulator of carotenoid (Xiong *et al.*, 2019) and anthocyanin (Luo *et al.*, 2021) accumulation through the direct interaction with the promoters of biosynthetic genes. Interestingly, both these pathways were strongly down-regulated in *Slhy5* mutant fruits. Although SlHY5 binds to the promoter of carotenoid and flavonoid biosynthetic genes (Wang *et al.*, 2021), no information was available regarding its direct effect on their transcriptional activation until now. In this sense, our data unravel a flavonoid accumulation mechanism in which SlBBX20 (Solyc12g089240) induces the expression of the biosynthetic genes that is synergistically enhanced by the presence of SlHY5 (Fig. 6). Moreover, SlHY5 itself can induce the transcriptional activity of the *SlBBX20* promoter, but not of flavonoid biosynthetic genes. Therefore, the previously reported flavonoid reduction in *Slhy5* mutant fruits is likely to be due to the down-regulation of *SlBBX20* (Wang *et al.*, 2021). Such a mechanism seems to be conserved in other species where the heterodimerization of BBXs and HY5 promotes flavonoid and anthocyanin accumulation, as described in *A. thaliana* (Bursch *et al.*, 2020) and *Pyrus pyrifolia* (Bai *et al.*, 2019).

The reduction of SGAs in *Slbbx20* ripe fruits also corroborates the synergistic interaction model between SlHY5 and BBX20 for the regulation of fruit metabolism (Supplementary Table S7). SGA levels were decreased but not abolished by the absence of SlBBX20. Similarly, loss of SlHY5 produced analogous effects to SGA accumulation (Zhang *et al.*, 2022). This evidence indicates that SlHY5 interacts with BBX20 to modulate the expression of the SGA pathway.

The antifungal effect of flavonoids has been extensively reported *in planta* and, in fruit and vegetable post-harvest resistance (Treutter, 2006). *Pyricularia oryzae* growth is inhibited by naringenin, kaempferol, and quercetin in decreasing order (Padmavati *et al.*, 1997). Protoanthocyanidins and dihydroquercetin are involved in barley resistance to *Fusarium* species (Skadhauge *et al.*, 1997), while quercetin and its derivatives inhibit *Neurospora crassa* growth (Parvez *et al.*, 2004). Furthermore, jasmonic acid (JA)-mediated SGA accumulation is known to repress fungal infection in tomato (Montero-Vargas *et al.*, 2018). It is known that light-mediated plant growth and defense response cross-talk in an intricate network (Pierik and Ballaré, 2021). In a direct way, low R/FR ratios suppress the formation of jasmonyl-L-isoleucine (JA-Ile), the bioactive conjugate of the defense hormone JA. This mechanism involves the PIF-mediated activation of a JA-catalyzing enzyme, resulting in the enhanced stability of JASMONATE-ZIM DOMAIN (JAZ) proteins and reduced defense response (Fernández-Milmanda *et al.*, 2020). In this context, although the exact function of SlBBX20 in the regulation of specialized metabolism and fruit defense must be further investigated, the susceptibility to *B. cinerea* observed in *Slbbx20* fruits (Fig. 7) might be partially due to reduced content of flavonoids and SGAs, as well as possibly alterations in JA production and signaling.

Altogether, the obtained data revealed that SlBBX20 is a positive regulator of light signaling that controls growth by limiting SlPIF4 activity. Afterwards, in an auxin-related manner, SlBBX20 coordinates cell division and expansion, ensuring a normal growth rate and, consequently, vegetative and reproductive development. Finally, the accumulation of SlBBX20 during ripening in response to SlRIN enhances fruit flavonoid content by the direct induction of the biosynthetic genes, which is boosted by SlBBX20–SlHY5 interaction. In summary, this work provides further evidence that manipulating BBXs is a suitable strategy for tailoring harvestable organ yield and quality (Fig. 8).

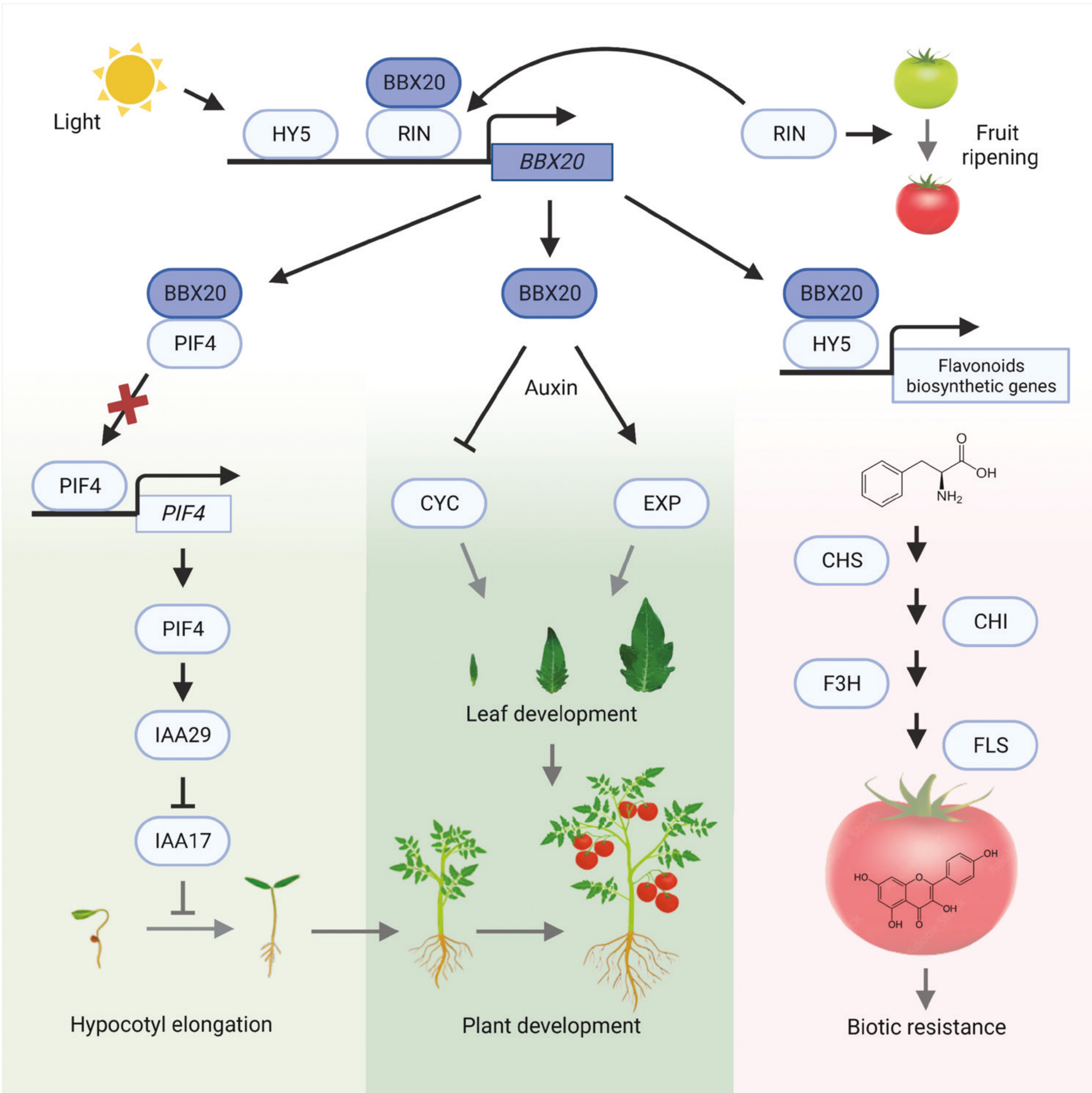

Fig. 8. SlBBX20 regulates several processes during plant development. SlBBX20 molecular mechanisms controlling tomato plant development and fruit quality. The binding of SlRIN to the *SlBBX20* promoter and of SlHY5 to the promoters of flavonoid biosynthetic genes was demonstrated through ChIP followed by qPCR (Lira *et al*., 2020; Wang *et al*., 2021, respectively). Abbreviations: ELONGATED HYPOCOTYL 5 (HY5), PHYTOCHROME INTERACTING FACTOR 4 (PIF4), AUXIN/INDOLE-3-ACETIC ACID (IAA29, IAA17), CYCLIN (CYC), EXPANSIN (EXP), RIPENING INHIBITOR (RIN), CHALCONE SYNTHASE 1 (CHS), CHALCONE ISOMERASE (CHI), FLAVANONE 3-HYDROXYLASE (F3H), and FLAVONOL SYNTHASE (FLS). Gray and black arrows indicate physiological processes and regulatory links, respectively. Bar/arrow line end represents negative/positive interactions. Created with BioRender.com.

Supplementary data

The following supplementary data are available at *JXB* online.

Table S1. Primers used in the experiments.

Table S2. Nuclear localization signals (NLSs) predicted in the SlBBX20 sequence.

Table S3. Relative transcript expression of cell division- and expansion-related genes in *Slbbx20* during leaf development.

Table S4. Carotenoid content in *Slbbx20* fruits.

Table S5. Flavonoid content in *Slbbx20* fruits.

Table S6. Relative transcript expression of flavonoid biosynthetic genes in *Slbbx20* fruits.

Table S7. Steroidal glycoalkaloid content in *Slbbx20* fruits.

Fig. S1. *SlBBX* expression during fruit development.

Fig. S2. SlBBX20 protein characterization.

Fig. S3. Characterization of the *Slbbx20* mutant.

Fig. S4. *Slbbx20* seedling response to light.

Fig. S5. *SlRIN* expression in *Slbbx20* fruits.

Fig. S6. Ripe fruits of the *Slbbx20* mutant show orangish color.

Acknowledgements

We thank Silvia Blanco and Amanda Ferreira Macedo for their technical support.

Author contributions

LS, JdRM, and BSL: performing most of the experiments, and data analysis; MJO, RTAW, GPCS, JLdSJ, EF, MJPF, and GGO: performing some experiments; EC and NN: performing the SGA metabolite profiling experiment and analysis; AG, JB, LF, and MR: conceptualization and design; LS, JdRM, BSL, and MR: writing the paper and collating the contributions of all authors. All authors read and approved the final manuscript. MR agrees to serve as the author responsible for contact and ensures communication.

Conflict of interest

The authors declare no conflict of interest.

Funding

LS, JRM, RTAW, and GP were recipients of FAPESP (Fundação de Amparo à Pesquisa do Estado de São Paulo, Brazil) fellowships. MJO, MJPF, LF, and MR were funded by fellowships from the CNPq (Conselho Nacional de Desenvolvimento Científico e Tecnológico, Brasil). JLSJ was the recipient of a CAPES (Coordenação de Aperfeiçoamento de Pessoal de Nível Superior, Brazil) fellowship. BSL was the recipient of a fellowship granted by GALY Company. This work was partially supported by grants from FAPESP 2016/01128-9 and 2021/0507-1 (Brazil), CAPES Finance Code 001 and USP (Universidade de São Paulo, Brazil), the Research Foundation Flanders (grants G0F6220N and G0E1122N), and the European Union's Horizon 2020 Research and Innovation Program under Grant Agreement no. 825730 (Endoscape).

Data availability

All primary data that support the findings of this work are freely available upon request.

References

An H, Roussot C, Suárez-López P, *et al*. 2004. CONSTANS acts in the phloem to regulate a systemic signal that induces photoperiodic flowering of *Arabidopsis*. Development **131**, 3615–3626.

Bai S, Tao R, Tang Y, *et al*. 2019. BBX16, a B-box protein, positively regulates light-induced anthocyanin accumulation by activating *MYB10* in red pear. Plant Biotechnology Journal **17**, 1985–1997.

Bemer M, Karlova R, Ballester AR, Tikunov YM, Bovy AG, Wolters-Arts M, de Barros Rossetto P, Angenent GC, de Maagd RA. 2012. The tomato FRUITFULL homologs TDR4/FUL1 and MBP7/FUL2 regulate ethylene-independent aspects of fruit ripening. The Plant Cell **24**, 4437–4451.

Ben-Naim O, Eshed R, Parnis A, Teper-Bamnolker P, Shalit A, Coupland G, Samach A, Lifschitz E. 2006. The CCAAT binding factor can mediate interactions between CONSTANS-like proteins and DNA. The Plant Journal **46**, 462–476.

Bianchetti R, Bellora N, de Haro LA, Zuccarelli R, Rosado D, Freschi L, Rossi M, Bermudez L. 2022. Phytochrome-mediated light perception affects fruit development and ripening through epigenetic mechanisms. Frontiers in Plant Science **13**, 870974.

Bursch K, Toledo-Ortiz G, Pireyre M, Lohr M, Braatz C, Johansson H. 2020. Identification of BBX proteins as rate-limiting cofactors of HY5. Nature Plants **6**, 921–928.

Cantu D, Blanco-Ulate B, Yang L, Labavitch JM, Bennett AB, Powell AL. 2009. Ripening-regulated susceptibility of tomato fruit to *Botrytis cinerea* requires *NOR* but not *RIN* or ethylene. Plant Physiology **150**, 1434–1449.

Cao J, Yuan J, Zhang Y, Chen C, Zhang B, Shi X, Niu R, Lin F. 2023. Multi-layered roles of BBX proteins in plant growth and development. Stress Biology **3**, 1.

Cao Y, Han Y, Meng D, Li D, Jiao C, Jin Q, Lin Y, Cai Y. 2017. B-BOX genes: genome-wide identification, evolution and their contribution to pollen growth in pear (*Pyrus bretschneideri* Rehd.). BMC Plant Biology **17**, 156.

Cao Y, Meng D, Han Y, Chen T, Jiao C, Chen Y, Jin Q, Cai Y. 2019. Comparative analysis of B-BOX genes and their expression pattern analysis under various treatments in *Dendrobium officinale*. BMC Plant Biology **19**, 245.

Čermák T, Curtin SJ, Gil-Humanes J, *et al*. 2017. A multipurpose toolkit to enable advanced genome engineering in plants. The Plant Cell **29**, 1196–1217.

Chang Y, Sun H, Liu S, *et al*. 2023. Identification of BBX gene family and its function in the regulation of microtuber formation in yam. BMC Genomics **24**, 354.

Chow C, Lee TY, Hung YC, Guan-Zhen L, Tseng KC, Liu YH, Kuo PL, Zheng HQ, Chang WC. 2019. PlantPAN3.0: a new and updated resource for reconstructing transcriptional regulatory networks from ChIP-seq experiments in plants. Nucleic Acids Research **47**, D1155–D1163.

Chu Z, Wang X, Li Y, Yu H, Li J, Lu Y, Li H, Ouyang B. 2016. Genomic organization, phylogenetic and expression analysis of the B-BOX gene family in tomato. Frontiers in Plant Science **7**, 1552.

Cober ER, Voldeng HD. 2001. Low R:FR light quality delays flowering of *E7E7* soybean lines. Crop Science **41**, 1823–1826.

Cookson SJ, Granier C. 2006. A dynamic analysis of the shade-induced plasticity in *Arabidopsis thaliana* rosette leaf development reveals new components of the shade-adaptative response. Annals of Botany **97**, 443–452.

Cruz AB, Bianchetti RE, Alves FRR, Purgatto E, Peres LEP, Rossi M, Freschi L. 2018. Light, ethylene and auxin signaling interaction regulates carotenoid biosynthesis during tomato fruit ripening. Frontiers in Plant Science **9**, 1370.

Cuéllar AP, Pauwels L, De Clercq R, Goossens A. 2013. Yeast two-hybrid analysis of jasmonate signaling proteins. Methods in Molecular Biology **1011**, 173–185.

Cui L, Zheng F, Wang J, *et al*. 2022. The tomato CONSTANS-LIKE protein SlCOL1 regulates fruit yield by repressing *SFT* gene expression. BMC Plant Biology **22**, 429.

Dahlin P, Müller MC, Ekengren S, McKee LS, Bulone V. 2017. The impact of steroidal glycoalkaloids on the physiology of *Phytophthora infestans*, the causative agent of potato late blight. Molecular Plant-Microbe Interactions **30**, 531–542.

de Wit M, Ljung K, Fankhauser C. 2015. Contrasting growth responses in lamina and petiole during neighbor detection depend on differential auxin responsiveness rather than different auxin levels. New Phytologist **208**, 198–209.

Dhar MK, Sharma R, Koul A, Kaul S. 2015. Development of fruit color in Solanaceae: a story of two biosynthetic pathways. Briefings in Functional Genomics **14**, 199–212.

Di Rienzo JA. 2009. Statistical software for the analysis of experiments of functional genomics. Argentina: RDNDA.

Di Rienzo JA, Casanoves F, Balzarini MG, Gonzalez L, Tablada M, Robledo YC. 2011. InfoStat versión 2011, Vo1. **8**. Argentina: Grupo InfoStat, FCA, Universidad Nacional de Córdoba, 195–199. http://www.infostat.com.ar

Elad Y. 1991. An inhibitor of polyamine biosynthesis—difluoromethylornithine—and the polyamine spermidine for the control of gray mold (*Botrytis cinerea*). Phytoparasitica **19**, 201–209.

Feng Z, Li M, Li Y, Yang X, Wei H, Fu X, Ma L, Lu J, Wang H, Yu S. 2021. Comprehensive identification and expression analysis of B-Box genes in cotton. BMC Genomics **22**, 439.

Fernández-Milmanda GL, Ballaré CL. 2021. Shade avoidance: expanding the color and hormone palette. Trends in Plant Science **26**, 509–523.

Fernández-Milmanda GL, Crocco CD, Reichelt M, *et al*. 2020. A light-dependent molecular link between competition cues and defence responses in plants. Nature Plants **6**, 223–230.

Fujisawa M, Nakano T, Shima Y, Ito Y. 2013. A large-scale identification of direct targets of the tomato MADS box transcription factor RIPENING INHIBITOR reveals the regulation of fruit ripening. The Plant Cell **25**, 371–386.

Gangappa SN, Botto JF. 2014. The BBX family of plant transcription factors. Trends in Plant Science **19**, 460–470.

Gehl C, Waadt R, Kudla J, Mendel RR, Hänsch R. 2009. New GATEWAY vectors for high throughput analyses of protein–protein interactions by bimolecular fluorescence complementation. Molecular Plant **2**, 1051–1058.

Gnesutta N, Kumimoto RW, Swain S, Chiara M, Siriwardana C, Horner DS, Holt BF, Mantovani R. 2017. CONSTANS imparts DNA sequence specificity to the histone fold NF-YB/NF-YC dimer. The Plant Cell **29**, 1516–1532.

Gomes GLB, Scortecci KC. 2021. Auxin and its role in plant development: structure, signalling, regulation and response mechanisms. Plant Biology (Stuttgart, Germany) **23**, 894–904.

Gommers CM, Visser EJ, St Onge KR, Voesenek LA, Pierik R. 2013. Shade tolerance: when growing tall is not an option. Trends in Plant Science **18**, 65–71.

Hoensch HP, Oertel R. 2015. The value of flavonoids for the human nutrition: short review and perspectives. Clinical Nutrition Experimental **3**, 8–14.

Hou W, Ren L, Zhang Y, Sun H, Shi T, Gu Y, Wang A, Ma D, Li Z, Zhang L. 2021. Characterization of BBX family genes and their expression profiles under various stresses in the sweet potato wild ancestor *Ipomoea trifida*. Scientia Horticulturae **288**, 110374.

Huang J, Zhao X, Weng X, Wang L, Xie W. 2012. The rice B-Box zinc finger gene family: genomic identification, characterization, expression profiling and diurnal analysis. PLoS One **7**, e48242.

Ito S, Ihara T, Tamura H, Tanaka S, Ikeda T, Kajihara H, Dissanayake C, Abdel-Motaal FF, El-Sayed MA. 2007. α-Tomatine, the major saponin in tomato, induces programmed cell death mediated by reactive oxygen species in the fungal pathogen *Fusarium oxysporum*. FEBS Letters **581**, 3217–3222.

James P, Halladay J, Craig EA. 1996. Genomic libraries and a host strain designed for highly efficient two-hybrid selection in yeast. Genetics **144**, 1425–1436.

Jin H, Xing M, Cai C, Li S. 2019. B-box proteins in *Arachis duranensis*: genome-wide characterization and expression profiles analysis. Agronomy **10**, 23.

Karimi M, Inzé D, Depicker A. 2002. GATEWAY™ vectors for *Agrobacterium*-mediated plant transformation. Trends in Plant Science **7**, 193–195.

Kosugi S, Hasebe M, Matsumura N, Takashima H, Miyamoto-Sato E, Tomita M, Yanagawa H. 2009. Six classes of nuclear localization signals specific to different binding grooves of importin α. Journal of Biological Chemistry **284**, 478–485.

Kurosaki H, Yumoto S. 2003. Effects of low temperature and shading during flowering on the yield components in soybeans. Plant Production Science **6**, 17–23.

Lee S, Zhu L, Huq E. 2021. An autoregulatory negative feedback loop controls thermomorphogenesis in *Arabidopsis*. PLoS Genetics **17**, e1009595.

Lira BS, Gramegna G, Trench BA, *et al*. 2017. Manipulation of a senescence-associated gene improves fleshy fruit yield. Plant Physiology **175**, 77–91.

Lira BS, Oliveira MJ, Shiose L, Vicente MH, Souza GPC, Floh EIS, Purgatto E, Nogueira FTS, Freschi L, Rossi M. 2022. SlBBX28 positively regulates plant growth and flower number in an auxin-mediated manner in tomato. Plant Molecular Biology **110**, 253–268.

Lira BS, Oliveira MJ, Shiose L, Wu RTA, Rosado D, Lupi ACD, Freschi L, Rossi M. 2020. Light and ripening-regulated BBX protein-encoding genes in *Solanum lycopersicum*. Scientific Reports **10**, 19235.

Liu X, Li R, Dai Y, Chen X, Wang X. 2018. Genome-wide identification and expression analysis of the B-box gene family in the apple (*Malus domestica* Borkh.) genome. Molecular Genetics and Genomics **293**, 303–315.

Luo D, Sun W, Cai J, Hu G, Zhang D, Zhang X, Yang C, Ye Z, Wang T. 2023. SlBBX20 attenuates JA signalling and regulates resistance to *Botrytis cinerea* by inhibiting SlMED25 in tomato. Plant Biotechnology Journal **21**, 792–805.

Luo D, Xiong C, Lin A, *et al*. 2021. SlBBX20 interacts with the COP9 signalosome subunit SlCSN5-2 to regulate anthocyanin biosynthesis by activating SlDFR expression in tomato. Horticulture Research **8**, 163.

Lykke-Andersen J, Bennett EJ. 2014. Protecting the proteome: eukaryotic cotranslational quality control pathways. Journal of Cell Biology **204**, 467–476.

Mohammed B, Bilooei SF, Dóczi R, Grove E, Railo S, Palme K, Ditengou FA, Bögre L, López-Juez E. 2018. Converging light, energy and hormonal signaling control meristem activity, leaf initiation, and growth. Plant Physiology **176**, 1365–1381.

Montero-Vargas JM, Casarrubias-Castillo K, Martínez-Gallardo N, Ordaz-Ortiz JJ, Délano-Frier JP, Winkler R. 2018. Modulation of steroidal glycoalkaloid biosynthesis in tomato (*Solanum lycopersicum*) by jasmonic acid. Plant Science **277**, 155–165.

Murashige T, Skoog F. 1962. A revised medium for rapid growth and bio assays with tobacco tissue cultures. Physiologia Plantarum **15**, 473–497.

Nguyen CV, Vrebalov JT, Gapper NE, Zheng Y, Zhong S, Fei Z, Giovannoni JJ. 2014. Tomato *GOLDEN2-LIKE* transcription factors reveal molecular gradients that function during fruit development and ripening. The Plant Cell **26**, 585–601.

Obel HO, Cheng C, Li Y, *et al*. 2022. Genome-wide identification of the B-Box gene family and expression analysis suggests their potential role in photoperiod-mediated β-carotene accumulation in the endocarp of cucumber (*Cucumis sativus* L.) fruit. Genes **13**, 658.

Padmavati M, Sakthivel N, Thara KV, Reddy AR. 1997. Differential sensitivity of rice pathogens to growth inhibition by flavonoids. Phytochemistry **46**, 499–502.

Pareja-Jaime Y, Roncero MIG, Ruiz-Roldán MC. 2008. Tomatinase from *Fusarium oxysporum* f. sp. *lycopersici* is required for full virulence on tomato plants. Molecular Plant-Microbe Interactions **21**, 728–736.

Parvez MM, Tomita-Yokotani K, Fujii Y, Konishi T, Iwashina T. 2004. Effects of quercetin and its seven derivatives on the growth of *Arabidopsis thaliana* and *Neurospora crassa*. Biochemical Systematics and Ecology **32**, 631–635.

Perrot-Rechenmann C. 2010. Cellular responses to auxin: division versus expansion. Cold Spring Harbor Perspectives in Biology **2**, a001446.

Pfaffl MW, Horgan GW, Dempfle L. 2002. Relative expression software tool (REST©) for group-wise comparison and statistical analysis of relative expression results in real-time PCR. Nucleic Acids Research **30**, e36.

Pierik R, Ballaré CL. 2021. Control of plant growth and defense by photoreceptors: from mechanisms to opportunities in agriculture. Molecular Plant **14**, 61–76.

Pierleoni A, Martelli PL, Fariselli P, Casadio R. 2006. BaCelLo: a balanced subcellular localization predictor. Bioinformatics **22**, e408–e416.

Pino LE, Lombardi-Crestana S, Azevedo MS, Scotton DC, Borgo L, Quecini V, Figueira A, Peres LE. 2010. The *Rg1* allele as a valuable tool for genetic transformation of the tomato 'Micro-Tom' model system. Plant Methods **6**, 23.

Pucciariello O, Legris MR, Rojas CC, *et al*. 2018. Rewiring of auxin signaling under persistent shade. Proceedings of the National Academy of Sciences, USA **115**, 5612–5617.

Putterill J, Robson F, Lee K, Simon R, Coupland G. 1995. The CONSTANS gene of *Arabidopsis* promotes flowering and encodes a protein showing similarities to zinc finger transcription factors. Cell **80**, 847–857.

Quadrana L, Almeida J, Otaiza SN, *et al*. 2013. Transcriptional regulation of tocopherol biosynthesis in tomato. Plant Molecular Biology **81**, 309–325.

Ruijter JM, Ramakers C, Hoogaars WMH, Karlen Y, Bakker O, Van den Hoff MJB, Moorman A. 2009. Amplification efficiency: linking baseline and bias in the analysis of quantitative PCR data. Nucleic Acids Research **37**, e45–e45.

Sandrock RW, VanEtten HD. 1998. Fungal sensitivity to and enzymatic degradation of the phytoanticipin α-tomatine. Phytopathology **88**, 137–143.

Schneider CA, Rasband WS, Eliceiri KW. 2012. NIH Image to ImageJ: 25 years of image analysis. Nature Methods **9**, 671–675.

Sérino S, Gomez L, Costagliola G, Gautier H. 2009. HPLC assay of tomato carotenoids: validation of a rapid microextraction technique. Journal of Agricultural and Food Chemistry **57**, 8753–8760.

Shalmani A, Jing XQ, Shi Y, Muhammad I, Zhou MR, Wei XY, Chen QQ, Li WQ, Liu WT, Chen KM. 2019. Characterization of B-BOX gene family and their expression profiles under hormonal, abiotic and metal stresses in Poaceae plants. BMC Genomics **20**, 1–22.

Shalmani A, Ullah U, Tai L, Zhang R, Jing XQ, Muhammad I, Bhanbhro N, Liu WT, Li WQ, Chen KM. 2023. OsBBX19–OsBTB97/OsBBX11 module regulates spikelet development and yield production in rice. Plant Science **334**, 111779.

Shan B, Bao G, Shi T, Zhai L, Bian S, Li X. 2022. Genome-wide identification of BBX gene family and their expression patterns under salt stress in soybean. BMC Genomics **23**, 1–17.

Silveira V, Balbuena TS, Santa-Catarina C, Floh EI, Guerra MP, Handro W. 2004. Biochemical changes during seed development in *Pinus taeda* L. Plant Growth Regulation **44**, 147–156.

Skadhauge B, Thomsen K, von Wettstein D. 1997. The role of barley testa layer and its flavonoid content in resistance to *Fusarium* infections. Hereditas **126**, 147–160.

Song J, Lin R, Tang M, Wang L, Fan P, Xia X, Yu J, Zhou Y. 2023. SlMPK1- and SlMPK2-mediated SlBBX17 phosphorylation positively regulates CBF-dependent cold tolerance in tomato. New Phytologist **239**, 1887–1902.

Song K, Li B, Wu H, Sha Y, Qin L, Chen X, Liu Y, Tang H, Yang L. 2022. The function of BBX gene family under multiple stresses in *Nicotiana tabacum*. Genes **13**, 1841.

Song Z, Heng Y, Bian Y, Xiao Y, Liu J, Zhao X, Jiang Y, Deng XW, Xu D. 2021. BBX11 promotes red light-mediated photomorphogenic development by modulating phyB-PIF4 signaling. Abiotech **2**, 117–130.

Song Z, Yan T, Liu J, Bian Y, Heng Y, Lin F, Jiang Y, Deng XW, Xu D. 2020. BBX28/BBX29, HY5 and BBX30/31 form a feedback loop to fine-tune photomorphogenic development. The Plant Journal **104**, 377–390.

Takeda F, Glenn DM, Callahan A, Slovin J, Stutte GW. 2010. Delaying flowering in short-day strawberry transplants with photoselective nets. International Journal of Fruit Science **10**, 134–142.

Talar U, Kiełbowicz-Matuk A. 2021. Beyond Arabidopsis: BBX regulators in crop plants. International Journal of Molecular Sciences **22**, 2906.

Talar U, Kiełbowicz-Matuk A, Czarnecka J, Rorat T. 2017. Genome-wide survey of B-box proteins in potato (*Solanum tuberosum*)—identification, characterization and expression patterns during diurnal cycle, etiolation and de-etiolation. PLoS One **12**, e0177471.

Thumuluri V, Almagro-Armenteros JJ, Johansen AR, Nielsen H, Winther O. 2022. DeepLoc 2.0: multi-label subcellular localization prediction using protein language models. Nucleic Acids Research **50**, W228–W234.

Tiwari SB, Shen Y, Chang HC, *et al*. 2010. The flowering time regulator CONSTANS is recruited to the *FLOWERING LOCUS T* promoter via a unique cis-element. New Phytologist **187**, 57–66.

Toledo-Ortiz G, Johansson H, Lee KP, Bou-Torrent J, Stewart K, Steel G, Rodríguez-Concepción M, Halliday KJ. 2014. The HY5–PIF regulatory module coordinates light and temperature control of photosynthetic gene transcription. PLoS Genetics **10**, e1004416.

Treutter D. 2006. Significance of flavonoids in plant resistance: a review. Environmental Chemistry Letters **4**, 147–157.

Tripathi P, Carvallo M, Hamilton EE, Preuss S, Kay SA. 2017. *Arabidopsis* B-BOX32 interacts with CONSTANS-LIKE3 to regulate flowering. Proceedings of the National Academy of Sciences, USA **114**, 172–177.

Vanden-Bossche R, Demedts B, Vanderhaeghen R, Goossens A. 2013. Transient expression assays in tobacco protoplasts. Methods in Molecular Biology **1011**, 227–239.

Vrebalov J, Ruezinsky D, Padmanabhan V, White R, Medrano D, Drake R, Schuch W, Giovannoni J. 2002. A MADS-box gene necessary for fruit ripening at the tomato *Ripening-Inhibitor* (*Rin*) locus. Science **296**, 343–346.

Wang CC, Meng LH, Gao Y, Grierson D, Fu DQ. 2018. Manipulation of light signal transduction factors as a means of modifying steroidal glycoalkaloids accumulation in tomato leaves. Frontiers in Plant Science **9**, 437.

Wang J, Yang G, Chen Y, *et al*. 2022. Genome-wide characterization and anthocyanin-related expression analysis of the *B-BOX* gene family in *Capsicum annuum* L. Frontiers in Genetics **13**, 847328.

Wang W, Wang P, Li X, Wang Y, Tian S, Qin G. 2021. The transcription factor SlHY5 regulates the ripening of tomato fruit at both the transcriptional and translational levels. Horticulture Research **8**, 82.

Wang Y, Zhai Z, Sun Y, *et al*. 2021a. Genome-wide identification of the B-BOX genes that respond to multiple ripening related signals in sweet cherry fruit. International Journal of Molecular Sciences **22**, 1622.

Wang Y, Zhang Y, Liu Q, Zhang T, Chong X, Yuan H. 2021b. Genome-wide identification and expression analysis of BBX transcription factors in *Iris germanica* L. International Journal of Molecular Sciences **22**, 8793.

Wei H, Wang P, Chen J, Li C, Wang Y, Yuan Y, Fang J, Leng X. 2020. Genome-wide identification and analysis of *B-BOX* gene family in grapevine reveal its potential functions in berry development. BMC Plant Biology **20**, 72.

Wu Y, Gong W, Yang W. 2017. Shade inhibits leaf size by controlling cell proliferation and enlargement in soybean. Scientific Reports **7**, 9259.

Wu Z, Fu D, Gao X, Zeng Q, Chen X, Wu J, Zhang N. 2023. Characterization and expression profiles of the B-box gene family during plant growth and under low-nitrogen stress in *Saccharum*. BMC Genomics **24**, 1–18.

Xiong C, Luo D, Lin A, *et al*. 2019. A tomato B-box protein SlBBX20 modulates carotenoid biosynthesis by directly activating *PHYTOENE SYNTHASE 1*, and is targeted for 26S proteasome-mediated degradation. New Phytologist **221**, 279–294.

Xu D, Jiang Y, Li J, Lin F, Holm M, Deng XW. 2016. BBX21, an *Arabidopsis* B-box protein, directly activates *HY5* and is targeted by COP1 for 26S proteasome-mediated degradation. Proceedings of the National Academy of Sciences, USA **113**, 7655–7660.

Xu D, Liu X, Guo C, Lin L, Yin R. 2023b. The B-box transcription factor 4 regulates seedling photomorphogenesis and flowering in tomato. Scientia Horticulturae **309**, 111692.

Xu D, Wang H, Feng X, Ma Y, Huang Y, Wang Y, Ding J, Chen H, Wu H. 2023a. Genome-wide identification, phylogenetic and expression analysis of the B-box gene family in the Woodland Strawberry (*Fragaria vesca*). Horticulturae **9**, 842.

Xu X, Wang Q, Li W, *et al*. 2022. Overexpression of SlBBX17 affects plant growth and enhances heat tolerance in tomato. International Journal of Biological Macromolecules **206**, 799–811.

Xuefen D, Wei X, Wang B, Xiaolin Z, Xian W, Jincheng L. 2022. Genome-wide identification and expression pattern analysis of quinoa BBX family. PeerJ **10**, e14463.

Yang G, Zhang C, Dong H, *et al*. 2022. Activation and negative feedback regulation of SlHY5 transcription by the SlBBX20/21–SlHY5 transcription factor module in UV-B signaling. The Plant Cell **34**, 2038–2055.

Zhang C, Wu Y, Liu X, Zhang J, Li X, Lin L, Yin R. 2022. Pivotal roles of ELONGATED HYPOCOTYL 5 in regulation of plant development and fruit metabolism in tomato. Plant Physiology **189**, 527–540.

Zhang Y, Mayba O, Pfeiffer A, Shi H, Tepperman JM, Speed TP, Quail PH. 2013. A quartet of PIF bHLH factors provides a transcriptionally centered signaling hub that regulates seedling morphogenesis through differential expression-patterning of shared target genes in *Arabidopsis*. PLoS Genetics **9**, e1003244.

Zhu Y, Zhu G, Xu R, Jiao Z, Yang J, Lin T, Wang Z, Huang S, Chong L, Zhu JK. 2023. A natural promoter variation of *SlBBX31* confers enhanced cold tolerance during tomato domestication. Plant Biotechnology Journal **21**, 1033–1043.

Zouine M, Maza E, Djari A, Lauvernier M, Frasse P, Smouni A, Pirrello J, Bouzayen M. 2017. TomExpress, a unified tomato RNA-Seq platform for visualization of expression data, clustering and correlation networks. The Plant Journal **92**, 727–735.